LA-UR-21-25245

Title:	A virtual element generalization on polygonal meshes of the Scott-Vogelius finite element method for the 2-D Stokes problem
Author(s):	Manzini, Gianmarco Mazzia, Annamaria
Intended for:	Report
Issued:	2021-06-02

A virtual element generalization on polygonal meshes of the Scott-Vogelius finite element method for the 2-D Stokes problem

G. Manzini [a] and A. Mazzia [b]

[a]*T-5 Applied Mathematics and Plasma Physics Group, Los Alamos National Laboratory, Los Alamos, NM 87545, USA*
[b]*Dipartimento di Ingegneria Civile, Edile e Ambientale - ICEA, Università di Padova, 35131 Padova, Italy*

Abstract

The virtual element method (VEM) is a Galerkin approximation method that extends the finite element method to polytopal meshes. In this paper, we present a conforming formulation that generalizes the Scott-Vogelius finite element method (FEM) for the numerical approximation of the Stokes problem to polygonal meshes in the framework of the virtual element method. In particular, we consider a straightforward application of the virtual element approximation space for scalar elliptic problems to the vector case and approximate the pressure variable through discontinuous polynomials. We assess the effectiveness of the numerical approximation by investigating the convergence on a manufactured solution problem and a set of representative polygonal meshes. We numerically show that this formulation is convergent with optimal convergence rates except for the lowest-order case on triangular and square meshes where the method coincides with the $\mathbb{P}_1 - \mathbb{P}_0$ Scott-Vogelius scheme, which is well-known to be unstable.

Key words: Virtual Element Method, Stokes Equations, Scott-Vogelius finite element method

1. Introduction

Many physical phenomena can be described using the system of incompressible Stokes equations as, for example, sedimentation and bio-suspension processes [58], droplet dynamics [60], micro-fluidic devices [71], fibrous filter design [62] and Stokes flows in porous media [7]. The Finite Element Method (FEM) was proven to be very successful in the numerical treatment of the Stokes equations in variational form, see [43, 53, 57]. Although the FEM is very effective, it is also limited to a very specific kind of unstructured meshes. In fact, the Partial Differential Equations (PDEs) are discretized by suitable polynomial trial and test functions that are conveniently built only on unstructured meshes of triangular and quadrilateral elements in two-dimensions (2-D) and tetrahedral and hexahedral elements in three dimensions (3-D). In the last decades, a great effort has been spent to overcome this limitation and to develop numerical methods for steady state and time-dependent problems working on more general polygonal and polyhedral meshes, [21, 61, 72–76].

The Mimetic Finite Difference (MFD) method [21, 63] was among the first effective approaches to be proposed in this direction. In fact, this numerical approach uses only the degrees of freedom without referring to any specific set of shape functions, and its design allows the numerical model to preserve several fundamental properties of the PDEs, such as maximum/minimum principles, solution symmetries and the conservation of mass, momentum and energy, see [44, 59]. Originally proposed for the numerical approximation of diffusion problems [40, 41], the MFD method was then extended to convection–diffusion problems [48], and Stokes equations [18–20].

The variational reformulation of the MFD method led to the Virtual Element Method (VEM) [8]. The VEM is a Galerkin method such as the finite element method where the approximation space in every mesh element is composed by the solutions of a differential problem. The basis functions of such Galerkin formulation exist as specific solutions of these elemental problems and they are uniquely identified by a special choice of the degrees of freedom. However, they are "virtual" as they are never built explicitly, and the bilinear forms of the variational formulation are approximated by using special polynomial projections that are computable from the degrees of freedom. The VEM is strictly related to the finite element formulations on polygonal and polyhedral meshes [49, 54, 64]. Strong connections also exist with other discretization methods that works on such kind of meshes, as for example the discontinuous skeletal gradient discretizations in [54], and the BEM-based FEM method in [47].

The first virtual element method was formulated as a conforming FEM for the Poisson problem [8], and then extended to convection-reaction-diffusion problems with variable coefficients [2, 15]. Similarly, the nonconforming formulation was proposed for the Poisson equation [6], and later extended to general elliptic problems [33, 50], Stokes problem [46], eigenvalue problems [55], and the biharmonic equation [4, 78]. The mixed virtual element method was proposed in [39] and [13] as the extension to the virtual element setting of the Brezzi-Douglas-Marini and Raviart-Thomas mixed methods [37]. The connection with the de Rham diagrams and the Nedelec elements and possible applications to electromagnetics have been explored in [12]. A (surely non-exhaustive) list of other significant applications of the VEM includes the works of References [3, 5, 9–17, 21–36, 42, 45, 51, 52, 66–69, 77].

In this work, we are interested in extending the Scott-Vogelius finite element method for the discretization of the 2D Stokes equation to the virtual element setting. The method that we present consider a discrete representation of the two components of the velocity field by using the conforming virtual element space originally proposed in [8, 9] and its modified ("enhanced") version proposed in [2]. The scalar unknown, e.g., the pressure, is approximated by discontinuous polynomials on the mesh elements. The resulting discretization at the lowest order case on triangular meshes coincides with the $\mathbb{P}_1 - \mathbb{P}_0$ Scott-Vogelius FEM. In such a case, the scheme can be non-convergent as the "inf-sup" stability condition cannot be ensured. However, in all other cases our VEM provides a different discretization, which performs well in the experiments we carried out. The zero divergence constraint is satisfied in a variational sense, i.e., the projection of the divergence on the subset of polynomials used in the scheme formulation is zero. It is worth mentioning that other virtual element approaches were recently proposed in the literature that approximate the Stokes velocity in such a way that its divergence is a polynomial that is set to zero in the scheme. This strategy provides an approximation of the Stokes velocity that satisfies the zero divergence constraint in a pointwise sense. We refer the interested reader to the works of References [17, 23, 24, 28]. However, the polynomial projection of the velocity divergence in our VEM is zero up to the machine precision. If we consider such projection as our numerical approximation to the velocity divergence, such approximation is identically zero in the computational domain.

The paper is organized as follows. The Stokes equations in strong and variational form are introduced in Section 2. The virtual element method and its connection with the Scott-Vogelius finite element method are presented and discussed in Section 3. The convergence behavior of our VEM is established in Section 4, where we derive an error estimate for both velocity and pressure in the energy norm, and investigated numerically in Section 5 through a manufactured solution test case that is solved on a set of representative polygonal meshes. This set of meshes includes also the triangular meshes where the low-order original Scott-Vogelius finite element method may show a well-known unstable behavior, thus allowing us to study the "inf-sup" stability of the method numerically. Final remarks and hints for future work are given in Section 6.

2. The Stokes problem and the virtual element discretization

2.1. *Notation and technicalities*

Consider the integer number $k > 0$ and let ω be a bounded, open, connected subset of $\mathbb{R}^2$. According to the notation and definitions given in [1], $L^2(\omega)$ is the linear space of square integrable functions defined on ω and $H^k(\omega)$, is the linear subspace of functions in $L^2(\omega)$ whose weak derivatives of order less than or equal to k are also in $L^2(\omega)$. We denote the norm and seminorm in $H^k(\omega)$ by $|| \cdot ||_{k,\omega}$ and $| \cdot |_{k,\omega}$, respectively. Throughout the paper, we prefer denoting the scalar product between scalar and vector-valued fields by the integral notation, even if sometimes we use

the notation "$(\cdot, \cdot)$" for the sake of conciseness.

In the formulation of the Stokes problem on the computational domain Ω, we use the linear space

$$L_0^2(\Omega) := \left\{ q \in L^2(\Omega) \ : \ \int_\Omega q \, d\mathbf{x} = 0 \right\}, \tag{1}$$

which is clearly a subspace of $L^2(\Omega)$. This subspace is isomorphic to the quotient space $L^2(\Omega)\backslash\mathbb{R}$, where two square integrable functions are equivalent and identified as members of the same equivalence class (which we still call "function") if their difference is constant.

2.2. *Strong and weak form of the Stokes problem*

We are interested in the numerical discretization of the system of incompressible Stokes equations

$$-\Delta\mathbf{u} + \nabla p = \mathbf{f} \quad \text{in } \Omega, \tag{2}$$

$$\text{div } \mathbf{u} = 0 \quad \text{in } \Omega, \tag{3}$$

for the velocity vector $\mathbf{u}$ and the pressure p defined on the computational domain Ω, which we assume to be an open, bounded, polygonal subset of $\mathbb{R}^2$, whose boundary is denoted by Γ. For the mathematical well-posedness of this problem, we consider the homogeneous Dirichlet boundary condition

$$\mathbf{u} = 0 \quad \text{on } \Gamma. \tag{4}$$

Assumption (4) makes the exposition simpler and immediate and is not restrictive on the design of the scheme as more general boundary conditions can be included with some additional technicalities. In particular, including nonhomogeneous Dirichlet boundary conditions is straightforward and this case will be considered in the numerical experiments.

To write the variational formulation of problem (2)-(4), we introduce the bilinear forms $a(\cdot, \cdot) : \left[H^1(\Omega)\right]^2 \times \left[H^1(\Omega)\right]^2 \to \mathbb{R}$ and $b(\cdot, \cdot) : \left[H^1(\Omega)\right]^2 \times L^2(\Omega) \to \mathbb{R}$:

$$a(\mathbf{v}, \mathbf{w}) := \int_\Omega \nabla\mathbf{v} : \nabla\mathbf{w} \, d\mathbf{x} \qquad \forall \mathbf{v}, \mathbf{w} \in \left[H^1(\Omega)\right]^2, \tag{5}$$

$$b(\mathbf{v}, q) := -\int_\Omega q \text{div } \mathbf{v} \, d\mathbf{x} \qquad \forall \mathbf{v} \in \left[H^1(\Omega)\right]^2, q \in L^2(\Omega). \tag{6}$$

The symbol ":" in (5) is the standard "dot" product between two-dimensional tensors. Now, the variational formulation is given by: *Find* $(\mathbf{u}, p) \in \left[H_0^1(\Omega)\right]^2 \times L_0^2(\Omega)$ such that

$$a(\mathbf{u}, \mathbf{v}) + b(\mathbf{v}, p) = (\mathbf{f}, \mathbf{v}) \qquad \forall \mathbf{v} \in \left[H_0^1(\Omega)\right]^2, \tag{7}$$

$$b(\mathbf{u}, q) = 0 \qquad \forall q \in L_0^2(\Omega). \tag{8}$$

The existence and uniqueness of the solution pair $(\mathbf{u}, p)$, cf. [37, 56, 57], follows on noting that the bilinear form $a(\cdot, \cdot)$ is continuous and coercive, and the bilinear form $b(\cdot, \cdot)$ is continuous and satisfies the inf-sup condition:

$$\inf_{q \in L_0^2(\Omega)} \sup_{\mathbf{v} \in [H_0^1(\Omega)]^2} \frac{b(\mathbf{v}, q)}{||\mathbf{v}||_{1,\Omega} \, ||q||_{0,\Omega}} \geq \beta,$$

for some real, strictly positive constant β.

We consider the two finite-dimensional approximation spaces $\mathbf{V}_k^h$ and $Q_{\underline{k}}^h$ for the vector and the scalar unknowns, where k and $\underline{k}$ are two integer numbers such that $\underline{k} \leq k - 1$. These spaces are labeled by h to indicate that they are built on a given mesh Ω_h. We assume that $\mathbf{V}_k^h$ is a conforming subspace of $\left[H_0^1(\Omega)\right]^2$ and $Q_{\underline{k}}^h$ a discontinuous subspace of $L_0^2(\Omega)$. We search for a vector field $\mathbf{u}_h \in \mathbf{V}_k^h$ and a scalar field $p_h \in Q_{\underline{k}}^h$ that approximates $\mathbf{u}$ and p, respectively. These fields are the solution of the following variational problem: *Find* $(\mathbf{u}_h, p_h) \in \mathbf{V}_k^h \times Q_{\underline{k}}^h$ such that

$$a_h(\mathbf{u}_h, \mathbf{v}_h) + b_h(\mathbf{v}_h, p_h) = \langle \mathbf{f}_h, \mathbf{v}_h \rangle \qquad \forall \mathbf{v}_h \in \mathbf{V}_k^h, \tag{9}$$

$$b_h(\mathbf{u}_h, q_h) = 0 \qquad \forall q_h \in Q_{\underline{k}}^h. \tag{10}$$

$$(\mathbf{k}, \underline{\mathbf{k}}) = (\mathbf{1}, \mathbf{0}) \qquad (\mathbf{k}, \underline{\mathbf{k}}) = (\mathbf{2}, \mathbf{1}) \qquad (\mathbf{k}, \underline{\mathbf{k}}) = (\mathbf{3}, \mathbf{2})$$
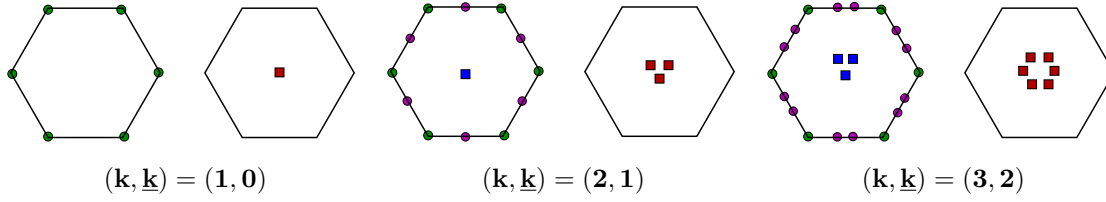
Fig. 1. Degrees of freedom of each component of the virtual element vector-valued fields of $\mathbf{V}_k^h(\mathrm{E})$ (left) and the scalar polynomial fields of $Q_{\underline{k}}^h(\mathrm{E})$ (right) of an hexagonal element for the accuracy degrees $k = 1, 2, 3$ and $\underline{k} = k - 1$. Nodal values are marked by a circular bullet; edge and cell polynomial moments are marked by a square bullet.

In equations (9) and (10) we use the virtual element approximations of the bilinear forms $a(\cdot, \cdot)$ and $b(\cdot, \cdot)$, which are denoted by $a_h(\cdot, \cdot) : \mathbf{V}_k^h \times \mathbf{V}_k^h \to \mathbb{R}$ and $b_h(\cdot, \cdot) : \mathbf{V}_k^h \times Q_{\underline{k}}^h \to \mathbb{R}$, respectively. Similarly, in in the right-hand side of equation (9) we use the virtual element approximations of the right-hand side of (7), here denoted by $\langle \mathbf{f}_h, \cdot \rangle$, where $\mathbf{f}_h$ is assumed to be an element of the dual space of $\mathbf{V}_k^h$.

3. The virtual element generalization of the Scott-Vogelius finite element method

3.1. *Mesh definition and regularity assumptions*

Let $\mathcal{T} = \{\Omega_h\}_h$ be a mesh family for Ω if every mesh Ω_h is a finite set of polygonal elements E such that $\overline{\Omega} = \cup_{\mathrm{E} \in \Omega_h} \overline{\mathrm{E}}$. Each mesh is labeled by the subindex h, which is, as usual, the maximum of the diameters of the mesh elements, i.e., $h_{\mathrm{E}} = \sup_{\mathbf{x}, \mathbf{y} \in \mathrm{E}} |\mathbf{x} - \mathbf{y}|$. We assume that all the elements of a given mesh are nonoverlapping in the sense that the intersection of the closure in $\mathbb{R}^2$ of any pair of them can only be a mesh vertex or a mesh edge. Therefore, the area of such intersection is zero. Every polygonal element E has $N_{\mathrm{E}}^{\mathcal{V}}$ vertices with coordinates $\mathbf{x}_{\mathsf{v}} = (x_{\mathsf{v}}, y_{\mathsf{v}})$. These vertices are connected by $N_{\mathrm{E}}^{\mathcal{E}}$ nonintersecting straight edges e, which form the boundary $\partial \mathrm{E}$. The measure of E is denoted by $|\mathrm{E}|$, its centroid (e.g., the barycenter) by $\mathbf{x}_{\mathrm{E}} := (x_{\mathrm{E}}, y_{\mathrm{E}})$, the unit outward vector orthogonal to the elemental edge e by $\mathbf{n}_{\mathrm{E}, \mathrm{e}}$. We also introduce the unit vector $\mathbf{n}_{\mathrm{e}}$, which is orthogonal to the edge e and whose orientation is independent of the elements E and fixed *once and for all* in the mesh. Note that for any given edge e, the vector $\mathbf{n}_{\mathrm{E}, \mathrm{e}}$ may differ from $\mathbf{n}_{\mathrm{e}}$ only by the multiplicative factor -1.

The mesh sequence used in the formulation of the method is required to satisfy the two following conditions: there exists a positive constant ϱ such that
– **(M1)** all polygonal elements E are star-shaped with respect to a disk with a radius, r, such that $r \geq \varrho h_{\mathrm{E}}$;
– **(M2)** all polygonal edges $\mathrm{e} \in \partial \mathrm{E}$ of all polygonal elements E satisfy $h_{\mathrm{e}} \geq \varrho h_{\mathrm{E}}$, where h_{e} is the edge length.
We assume that ϱ is independent of h, so that these regularity assumptions are uniformly satisfied by all the meshes Ω_h of the mesh family $\mathcal{T} = \{\Omega_h\}_h$ used in the VEM formulation. Property **(M1)** implies that all the mesh elements are *simply connected* subsets of $\mathbb{R}^2$. Property **(M2)** implies that the number of edges in the elemental boundaries is uniformly bounded over the whole mesh family $\mathcal{T}$. We remark that under these conditions the theory of polynomial approximation of functions in Sobolev spaces [38] provides interpolation and projection error estimates that can be used in the analysis of the method.

3.2. *Scalar and vector approximation spaces*

If E is a generic mesh element and ℓ a nonnegative integer number, we let $\mathbb{P}_\ell(\mathrm{E})$ denote the linear space of polynomials of degree up to ℓ defined on E, with the useful convention that $\mathbb{P}_{-1}(\mathrm{E}) = \{0\}$, and $[\mathbb{P}_\ell(\mathrm{E})]^2$ denotes the space of two-dimensional vector polynomials of degree up to ℓ on E. We use the notation $\mathbb{P}_\ell(\Omega_h)$ for the elementwise polynomials of degree ℓ defined on the mesh Ω_h, so that $q \in \mathbb{P}_\ell(\Omega_h)$ is such that $q_{|\mathrm{E}} \in \mathbb{P}_\ell(\mathrm{E})$ for all $\mathrm{E} \in \Omega_h$. Similarly, if e is a generic mesh edge, we let $\mathbb{P}_\ell(\mathrm{e})$ denote the linear space of polynomials of degree up to ℓ defined on e.

For the approximation of the scalar unknown p, we consider the functional space of discontinuous polynomials of degree $\underline{k}$ having zero average defined on the mesh Ω_h, which we formally define as $Q_{\underline{k}}^h := \mathbb{P}_{\underline{k}}(\Omega_h) \cap L_0^2(\Omega)$.

4

Instead, for the approximation of the vector unknown $\mathbf{u}$ we consider the functional space of vector-valued functions

$$\mathbf{V}_k^h := \left\{ \mathbf{v}_h \in \left[H_0^1(\Omega)\right]^2 \, : \, \mathbf{v}_{h|\mathrm{E}} \in \mathbf{V}_k^h(\mathrm{E}) \quad \forall \mathrm{E} \in \Omega_h \right\}, \qquad k \geq 1, \tag{11}$$

which is a conforming finite-dimensional subspace of $\left[H_0^1(\Omega)\right]^2$. This functional space is defined by gluing together the local virtual element spaces $\mathbf{V}_k^h(\mathrm{E})$ defined on the mesh elements $\mathrm{E} \in \Omega_h$. We take $\mathbf{V}_k^h(\mathrm{E}) = \left[V_k^h(\mathrm{E})\right]^2$ where $V_k^h(\mathrm{E})$ is either the scalar virtual element space originally introduced in [8]

$$V_k^h(\mathrm{E}) := \left\{ v_h \in H^1(\mathrm{E}) \, : \, v_{h|\partial\mathrm{E}} \in C^0(\partial\mathrm{E}), \, v_{h|\mathrm{e}} \in \mathbb{P}_k(\mathrm{e}) \, \forall \mathrm{e} \in \partial\mathrm{E}, \, \Delta v_h \in \mathbb{P}_{k-2}(\mathrm{E}) \right\}, \tag{12}$$

or its "modified" version (also called "enhanced" in the virtual element literature) given by [2]

$$V_k^h(\mathrm{E}) := \left\{ v_h \in H^1(\mathrm{E}) \, : v_{h|\partial\mathrm{E}} \in C^0(\partial\mathrm{E}), \, v_{h|\mathrm{e}} \in \mathbb{P}_k(\mathrm{e}) \, \forall \mathrm{e} \in \partial\mathrm{E}, \, \Delta v_h \in \mathbb{P}_k(\mathrm{E}), \right.$$
$$\left. \int_{\mathrm{E}} \left(v_h - \Pi_k^{\nabla,\mathrm{E}} v_h\right) q \, d\mathbf{x} = 0 \quad \forall q \in \mathbb{P}_k(\mathrm{E}) \backslash \mathbb{P}_{k-2}(\mathrm{E}) \right\}, \tag{13}$$

where $\mathbb{P}_k(\mathrm{E}) \backslash \mathbb{P}_{k-2}(\mathrm{E})$ is the space of polynomials of degree exactly equal to k or $k-1$. To avoid the multiplication of symbols practically denoting the same thing, we use the notation "V_k^h" for the spaces in (12) and (13) with a minor abuse of notation. The definition of the virtual element vector space in (13) has been modified according to the so-called *enhancement strategy*, so that the L^2-orthogonal projection onto $\left[\mathbb{P}_k(\mathrm{E})\right]^2$ of a virtual element function $\mathbf{v}_h \in \mathbf{V}_k^h(\mathrm{E})$ is computable.

Remark 3.1 (Connection with the Scott-Vogelius finite element method) *The approximation spaces defined above contains the Scott-Vogelius finite element method as a special case. In fact, if we consider a triangular mesh, we recover the Scott-Vogelius FEM by setting $\mathbf{V}_k^h = \mathbf{V}_k^{SV,h}$, where*

$$\mathbf{V}_k^{SV,h} := \left\{ \mathbf{v}_h \in \left[H^1(\Omega)\right]^2 \, : \, \mathbf{v}_{h|E} \in \left[\mathbb{P}_k(E)\right]^2 \quad \forall E \in \Omega_h \right\}, \tag{14}$$

$$Q_{\underline{k}}^h := \left\{ q_h \in L_0^2(\Omega) \, : \, q_{h|E} \in \mathbb{P}_{\underline{k}}(E) \quad \forall E \in \Omega_h \right\} = \mathbb{P}_{\underline{k}}(\Omega_h) \cap L_0^2(\Omega), \tag{15}$$

for $k \geq 1$ and $\underline{k} \leq k-1$, and taking $a_h(\cdot,\cdot) = a(\cdot,\cdot)$, $b_h(\cdot,\cdot) = b(\cdot,\cdot)$ in (9)-(10). It is well-known that the scheme with $k = 1$ and $\underline{k} = 0$ can be unstable on triangular and square meshes. It is worth noting that our virtual element method coincides with such approximations only on triangular and square meshes and only for $k = 1$ and $\underline{k} = 0$. In all the other cases, including for example $k = 2$ and $\underline{k} = 0$, our approach provides a different and well-behaving discretization. The performance of the VEM for different values of the integer pair $(k, \underline{k})$ on triangular and square meshes is investigated in the numerical section. Our numerical evidence shows that the VEM is stable and convergent except for the possibly unstable cases mentioned above.

3.3. *Degrees of freedom and polynomial projection operators*

The functions in the virtual element spaces (12) and the enhanced space (13) are uniquely characterized by the following set of values, the *degrees of freedom*:

$(\mathbf{D1})$ for $k \geq 1$, the vertex values $v_h(\mathbf{x}_\mathsf{v})$, $\mathsf{v} \in \partial\mathrm{E}$;

$(\mathbf{D2})$ for $k \geq 2$, the polynomial edge moments

$$\frac{1}{|\mathrm{e}|} \int_\mathrm{e} v_h(s) q_h(s) \, ds \qquad \forall q_h \in \mathbb{P}_{k-2}(\mathrm{e}) \tag{16}$$

for every edge $\mathrm{e} \in \partial\mathrm{E}$;

$(\mathbf{D3})$ for $k \geq 2$, the polynomial cell moments

$$\frac{1}{|\mathrm{E}|} \int_\mathrm{E} v_h(\mathbf{x}) q_h(\mathbf{x}) \, d\mathbf{x} \qquad \forall q_h \in \mathbb{P}_{k-2}(\mathrm{E}). \tag{17}$$

The unisolvence of $(\mathbf{D1})$-$(\mathbf{D3})$ is proved in Reference [8] for the space defined in (12), and in Reference [2] for the enhanced space defined in (13). In Figure 1, we illustrate the degrees of freedom for each velocity component and the scalar field for the polynomial degree $k = 1, 2, 3$ on an hexagonal element. The degrees of freedom that uniquely characterize the virtual element functions in the global space $\mathbf{V}_k^h$ are obtained by collecting the elemental degrees of freedom. Their unisolvence in the global space $\mathbf{V}_k^h$ is an immediate consequence of the unisolvence of the degrees of freedom $(\mathbf{D1})$-$(\mathbf{D3})$ in the elemental spaces $\mathbf{V}_k^h(\mathrm{E})$.

Remark 3.2 (Alternative choice of the degrees of freedom) *Instead of $(\mathbf{D2})$, we can select the values at a set of $k - 1$ internal nodes on each edge, e.g., the nodes supporting a one-dimensional Gauss-Lobatto integration rule with $k - 1$ internal nodes. This alternative choice is equivalent to $(\mathbf{D2})$. In the preliminary stages of our work, we carried out all numerical experiments with both choices of edge degrees of freedom and we did not find any significant difference in the results.*

Let v_h be a scalar virtual element function on the element E according to the definition given in (12) or (13). Then, the following polynomial projections are computable using the degrees of freedom $(\mathbf{D1})$-$(\mathbf{D3})$:

– the elliptic projection $\Pi_k^{\nabla,\mathrm{E}} v_h \in \mathbb{P}_k(\mathrm{E})$, which is the solution of the variational problem

$$\int_{\mathrm{E}} \nabla\big(v_h - \Pi_k^{\nabla,\mathrm{E}} v_h\big) q \, d\mathbf{x} = 0 \qquad \forall q \in \mathbb{P}_k(\mathrm{E}),$$

$$\int_{\partial\mathrm{E}} \big(v_h - \Pi_k^{\nabla,\mathrm{E}} v_h\big) \, ds = 0;$$

– the orthogonal projection $\Pi_{\bar{k}}^{0,\mathrm{E}} v_h \in \mathbb{P}_{\bar{k}}(\mathrm{E})$, which is the solution of the variational problem

$$\int_{\mathrm{E}} \big(v_h - \Pi_{\bar{k}}^{0,\mathrm{E}} v_h\big) q \, d\mathbf{x} = 0 \qquad \forall q \in \mathbb{P}_{\bar{k}}(\mathrm{E}),$$

where $\bar{k} = k - 2$ for $k \geq 2$ if $V_k^h(\mathrm{E})$ is defined by (12), and $\bar{k} = k \geq 1$ if $\mathbf{V}_k^h(\mathrm{E})$ is defined by (13).

Likewise, if $\mathbf{v}_h = (v_x, v_y)^T$ is a vector-valued field whose components are in the virtual element spaces defined by (12) or (13), the following projectors are computable:

– the orthogonal projection $\Pi_{\bar{k}}^{0,\mathrm{E}} \mathbf{v}_h$ of a vector-valued field $\mathbf{v}_h = (v_x, v_y)^T$, which is the solution of the variational problem

$$\int_{\mathrm{E}} \big(\mathbf{v}_h - \Pi_{\bar{k}}^{0,\mathrm{E}} \mathbf{v}_h\big) \cdot \mathbf{q} \, d\mathbf{x} = 0 \qquad \forall \mathbf{q} \in \big[\mathbb{P}_{\bar{k}}(\mathrm{E})\big]^2,$$

where $\bar{k} = k - 2$ for $k \geq 2$ if each component of $\mathbf{v}_h$ belongs to the scalar virtual element space $V_k^h(\mathrm{E})$ defined by (12), and $\bar{k} = k \geq 1$ if each component of $\mathbf{v}_h$ belongs to the enhanced virtual element space $V_k^h(\mathrm{E})$ defined by (13). The projection operator is computed component-wisely, i.e., $\Pi_{\bar{k}}^{0,\mathrm{E}} \mathbf{v}_h = (\Pi_{\bar{k}}^{0,\mathrm{E}} v_x, \Pi_{\bar{k}}^{0,\mathrm{E}} v_y)^T \in \big[\mathbb{P}_{\bar{k}}(\mathrm{E})\big]^2$, where $\Pi_{\bar{k}}^{0,\mathrm{E}} v_x$ and $\Pi_{\bar{k}}^{0,\mathrm{E}} v_y$ are the scalar orthogonal projections defined above;

– the orthogonal projection $\Pi_{k-1}^{0,\mathrm{E}} \nabla\mathbf{v}_h \in \big[\mathbb{P}_{k-1}(\mathrm{E})\big]^{2\times 2}$ of $\nabla\mathbf{v}_h$, the gradient of the virtual element vector-valued field $\mathbf{v}_h$, onto the linear space of the 2×2-sized matrix-valued polynomials of degree $\bar{k}$. These quantities are defined component-wisely as follows:

$$\nabla\mathbf{v}_h = \begin{pmatrix} \dfrac{\partial v_x}{\partial x} & \dfrac{\partial v_x}{\partial y} \\[2mm] \dfrac{\partial v_y}{\partial x} & \dfrac{\partial v_y}{\partial y} \end{pmatrix} \quad \text{and} \quad \Pi_{k-1}^{0,\mathrm{E}} \nabla\mathbf{v}_h = \begin{pmatrix} \Pi_{k-1}^{0,\mathrm{E}} \dfrac{\partial v_x}{\partial x} & \Pi_{k-1}^{0,\mathrm{E}} \dfrac{\partial v_x}{\partial y} \\[2mm] \Pi_{k-1}^{0,\mathrm{E}} \dfrac{\partial v_y}{\partial x} & \Pi_{k-1}^{0,\mathrm{E}} \dfrac{\partial v_y}{\partial y} \end{pmatrix}, \tag{18}$$

and this latter one is the solution of the variational problem:

$$\int_{\mathrm{E}} \big(\nabla\mathbf{v}_h - \Pi_{k-1}^{0,\mathrm{E}} \nabla\mathbf{v}_h\big) : \boldsymbol{\kappa} \, d\mathbf{x} = 0 \qquad \forall \boldsymbol{\kappa} \in \big[\mathbb{P}_{k-1}(\mathrm{E})\big]^{2\times 2}.$$

The computability of the scalar polynomial projection is proved in [2, 8], while the computability of the vector polynomial projection can easily be proved by using the same arguments of these papers component-wisely.

3.4. The virtual element bilinear forms $a_h(\cdot,\cdot)$

First, we note that the linearity of the integral in (5) allows us to split the bilinear forms $a(\cdot,\cdot)$ as a summation of the local bilinear forms defined on the mesh elements:

$$a(\mathbf{v},\mathbf{w}) = \sum_{\mathrm{E}\in\Omega_h} a^{\mathrm{E}}(\mathbf{v},\mathbf{w}) \quad \text{with} \quad a^{\mathrm{E}}(\mathbf{v},\mathbf{w}) = \int_{\mathrm{E}} \nabla\mathbf{v} : \nabla\mathbf{w}\,d\mathbf{x}, \tag{19}$$

$$\tag{20}$$

The virtual element bilinear form $a_h(\cdot,\cdot)$ can be defined as the sum of the local bilinear forms $a_h^{\mathrm{E}}(\cdot,\cdot) : \mathbf{V}_k^h(\mathrm{E}) \times \mathbf{V}_k^h(\mathrm{E}) \to \mathbb{R}$ by using the orthogonal projection operators:

$$a_h(\mathbf{v}_h,\mathbf{w}_h) = \sum_{\mathrm{E}\in\Omega_h} a_h^{\mathrm{E}}(\mathbf{v}_h,\mathbf{w}_h) \tag{21}$$

where

$$a_h^{\mathrm{E}}(\mathbf{v}_h,\mathbf{w}_h) = \int_{\mathrm{E}} \Pi_{k-1}^{0,\mathrm{E}}\nabla\mathbf{v}_h : \Pi_{k-1}^{0,\mathrm{E}}\nabla\mathbf{w}_h\,d\mathbf{x} + S_h\big((1-\Pi_k^{\mathrm{E}})\mathbf{v}_h,(1-\Pi_k^{\mathrm{E}})\mathbf{w}_h\big), \tag{22}$$

where Π_k^{E} can be either the orthogonal or the elliptic projection $\Pi_k^{0,\mathrm{E}}$ or $\Pi_k^{\nabla,\mathrm{E}}$. The definition in (22) includes the stabilization term provided by the local bilinear form $S_h(\cdot,\cdot) : \mathbf{V}_k^h(\mathrm{E}) \times \mathbf{V}_k^h(\mathrm{E}) \to \mathbb{R}$. According to the virtual element setting, for $S_h(\cdot,\cdot)$ we can choose any symmetric, positive definite bilinear form such that

$$\sigma_* a(\mathbf{v}_h,\mathbf{v}_h) \le S_h(\mathbf{v}_h,\mathbf{v}_h) \le \sigma^* a(\mathbf{v}_h,\mathbf{v}_h) \qquad \forall \mathbf{v}_h \in \mathbf{V}_k^h(\mathrm{E}) \cap \ker(\Pi_k^{\mathrm{E}}),$$

where σ_* and σ^* are two real, positive constants independent of h. A detailed study of possible stabilization forms can be found in [65]. This design is such that the following two fundamental properties are true for the local bilinear form $a_h^{\mathrm{E}}(\cdot,\cdot)$:

– **Stability**: there exist two real, positive constants α_* and α^* such that

$$\alpha_* a^{\mathrm{E}}(\mathbf{v}_h,\mathbf{v}_h) \le a_h^{\mathrm{E}}(\mathbf{v}_h,\mathbf{v}_h) \le \alpha^* a^{\mathrm{E}}(\mathbf{v}_h,\mathbf{v}_h) \qquad \forall \mathbf{v}_h \in \mathbf{V}_k^h(\mathrm{E}). \tag{23}$$

These constants are independent of h but can depend on other parameters of the discretization, such as ρ, which is related to the regularity of the mesh, σ_* and σ^*, and the order of the method k.

– **Polynomial consistency**: the *exactness property* holds

$$a_h^{\mathrm{E}}(\mathbf{v}_h,\mathbf{p}) = a^{\mathrm{E}}(\mathbf{v},\mathbf{p}), \tag{24}$$

for every vector field $\mathbf{v}_h \in \mathbf{V}_k^h(\mathrm{E})$ and vector polynomial field $\mathbf{q} \in \big[\mathbb{P}_k(\mathrm{E})\big]^2$.

These properties have two important consequences. First, adding all the local left inequalities in (23) implies that the bilinear form $a_h(\cdot,\cdot)$ is coercive on $\mathbf{V}_k^h \times \mathbf{V}_k^h$:

$$a_h(\mathbf{v}_h,\mathbf{v}_h) \ge \alpha_* |\mathbf{v}_h|_{1,\Omega}^2. \tag{25}$$

Second, the local bilinear form $a_h^{\mathrm{E}}(\cdot,\cdot)$ is continuous on $\mathbf{V}_k^h(\mathrm{E}) \times \mathbf{V}_k^h(\mathrm{E})$. Indeed, relation (23) and the symmetry of $a_h^{\mathrm{E}}(\cdot,\cdot)$ imply that $a_h^{\mathrm{E}}(\cdot,\cdot)$ is a semi-inner product on $\mathbf{V}_k^h(\mathrm{E})$ (indeed, it is an inner product on the quotient space $\mathbf{V}_k^h(\mathrm{E})\backslash\mathbb{R}^2$). Using the Cauchy-Schwarz inequality we find that:

$$a_h^{\mathrm{E}}(\mathbf{v}_h,\mathbf{w}_h) \le \big[a_h^{\mathrm{E}}(\mathbf{v}_h,\mathbf{v}_h)\big]^{\frac{1}{2}}\big[a_h^{\mathrm{E}}(\mathbf{w}_h,\mathbf{w}_h)\big]^{\frac{1}{2}} \le \alpha^* \big[a^{\mathrm{E}}(\mathbf{v}_h,\mathbf{v}_h)\big]^{\frac{1}{2}}\big[a^{\mathrm{E}}(\mathbf{w}_h,\mathbf{w}_h)\big]^{\frac{1}{2}}$$

$$= \alpha^* |\mathbf{v}_h|_{1,\mathrm{E}}|\mathbf{w}_h|_{1,\mathrm{E}}. \tag{26}$$

Then, we sum all the local inequalities and use again the Cauchy-Schwarz inequality and the right inequality of (23) to find that

$$\sum_{\mathrm{E}\in\Omega_h} a_h^{\mathrm{E}}(\mathbf{v}_h,\mathbf{w}_h) = \alpha^* \sum_{\mathrm{E}\in\Omega_h} |\mathbf{v}_h|_{1,\mathrm{E}}|\mathbf{w}_h|_{1,\mathrm{E}} \le \alpha^* \bigg(\sum_{\mathrm{E}\in\Omega_h} |\mathbf{v}_h|_{1,\mathrm{E}}^2\bigg)^{\frac{1}{2}}\bigg(\sum_{\mathrm{E}\in\Omega_h} |\mathbf{w}_h|_{1,\mathrm{E}}^2\bigg)^{\frac{1}{2}}$$

$$= \alpha^* |\mathbf{v}_h|_{1,\Omega}|\mathbf{w}_h|_{1,\Omega}, \tag{27}$$

which implies the global continuity of a_h.

3.5. *The virtual element bilinear forms* $b_h(\cdot, \cdot)$

First, we note that the linearity of the integral in (6) allows us to split the bilinear form $b(\cdot, \cdot)$ as a summation of the local bilinear forms defined on the mesh elements:

$$b(\mathbf{v}, q) = \sum_{\mathrm{E} \in \Omega_h} b^{\mathrm{E}}(\mathbf{v}, \mathbf{w}) \quad \text{with} \quad b^{\mathrm{E}}(\mathbf{v}, q) = -\int_{\mathrm{E}} q \operatorname{div} \mathbf{v} \, d\mathbf{x}. \tag{28}$$

We split $b_h(\cdot, \cdot)$ as the sum of the local bilinear forms $b_h^{\mathrm{E}}(\cdot, \cdot) : \mathbf{V}_k^h(\mathrm{E}) \times \mathbb{P}_{\underline{k}}(\mathrm{E}) \to \mathbb{R}$ to define its virtual element approximation:

$$b_h(\mathbf{v}_h, q) = \sum_{\mathrm{E} \in \Omega_h} b_h^{\mathrm{E}}(\mathbf{v}_h, q) \qquad \text{where} \qquad b_h^{\mathrm{E}}(\mathbf{v}_h, q) = \int_{\mathrm{E}} q \, \Pi_{\underline{k}}^{0,\mathrm{E}} \operatorname{div} \mathbf{v}_h \, d\mathbf{x}. \tag{29}$$

It holds that $b_h^{\mathrm{E}}(\mathbf{v}_h, q) = b^{\mathrm{E}}(\mathbf{v}_h, q)$ for every vector-valued field $\mathbf{v}_h \in \mathbf{V}_k^h(\mathrm{E})$ and polynomial scalar function $q \in \mathbb{P}_{\underline{k}}(\mathrm{E})$, where we recall that $b^{\mathrm{E}}(\cdot, \cdot)$ is defined in (28). This property is a straightforward consequence of the definition of the orthogonal projection operator $\Pi_{\underline{k}}^{0,\mathrm{E}}$. If we add this relation over all the mesh elements, we find that

$$b_h(\mathbf{v}_h, q) = b(\mathbf{v}_h, q) \qquad \forall \mathbf{v}_h \in \mathbf{V}_k^h, \, q \in \mathbb{P}_{\underline{k}}(\Omega_h) \tag{30}$$

for all pairs $(k, \underline{k})$ with $\underline{k} \le k - 1$, which can be used to simplify the implementation of the method.

3.6. *The virtual element approximation of the right-hand side*

Let $\bar{k}$ be a nonnegative integer number. The right hand-side of equation (9) is written as

$$\langle \mathbf{f}_h, \mathbf{v}_h \rangle = \sum_{\mathrm{E} \in \Omega_h} \int_{\mathrm{E}} \Pi_{\bar{k}}^{0,\mathrm{E}} \mathbf{f} \cdot \mathbf{v}_h \, d\mathbf{x} = \sum_{\mathrm{E} \in \Omega_h} \int_{\mathrm{E}} \mathbf{f} \cdot \Pi_{\bar{k}}^{0,\mathrm{E}} \mathbf{v}_h \, d\mathbf{x}, \tag{31}$$

where the vector-valued source term $\mathbf{f}$ is locally approximated by its orthogonal projection $\Pi_{\bar{k}}^{0,\mathrm{E}} \mathbf{f}$ onto the polynomial space $\mathbb{P}_{\bar{k}}(\mathrm{E})$ for all polygonal elements E. Note that we use the definition of the orthogonal projector $\Pi_{\bar{k}}^{0,\mathrm{E}}$ in the second equality above.

Two choices of $\bar{k}$ are possible:
- $\bar{k} = \max(0, k - 2)$ if we consider the virtual element space in (12);
- $\bar{k} = k$ (or $k - 1$): if we consider the enhanced virtual element space in (13).

The first choice was proposed for $k \ge 2$ in the original paper [8]. It is worth mentioning that for $k = 1$ the projector $\Pi_0^{0,\mathrm{E}}$ is substituted by the arithmetic average of the elemental vertex values for each velocity vector component. This choice allows us to obtain the correct convergence rate for the approximation of the velocity field in the energy norm. The second choice was proposed in Ref. [2] and allows us to obtain the correct convergence rate for the approximation of the velocity field in the L^2-norm.

We recall the error estimates pertaining these two possible approximations of the right-hand side, which follow on noting that $\left(1 - \Pi_{\bar{k}}^{0,\mathrm{E}}\right)$ is orthogonal to $\Pi_0^{0,\mathrm{E}}$ in the L^2-inner product. Assuming that $\mathbf{f} \in \left[H^{\bar{k}+1}(\Omega)\right]^2$ with $\bar{k} \ge 0$ we find that [8]:

$$|\langle \mathbf{f}_h, \mathbf{v}_h \rangle - (\mathbf{f}, \mathbf{v}_h)| = \left| \sum_{\mathrm{E} \in \Omega_h} \int_{\mathrm{E}} \left(\Pi_{\bar{k}}^{0,\mathrm{E}} \mathbf{f} - \mathbf{f}\right) \mathbf{v}_h \, d\mathbf{x} \right| \le \left| \sum_{\mathrm{E} \in \Omega_h} \int_{\mathrm{E}} \left(\Pi_{\bar{k}}^{0,\mathrm{E}} \mathbf{f} - \mathbf{f}\right) \left(\mathbf{v}_h - \Pi_0^{0,\mathrm{E}} \mathbf{v}_h\right) d\mathbf{x} \right|$$

$$\le \sum_{\mathrm{E} \in \Omega_h} ||\Pi_{\bar{k}}^{0,\mathrm{E}} \mathbf{f} - \mathbf{f}||_{0,\mathrm{E}} \, ||\mathbf{v}_h - \Pi_0^{0,\mathrm{E}} \mathbf{v}_h||_{0,\mathrm{E}} \le C h^{\bar{k}+2} ||\mathbf{f}||_{\bar{k}+1,\mathrm{E}} \, |\mathbf{v}_h|_{1,\mathrm{E}}, \tag{32}$$

for some constant $C > 0$ independent of h. For $\bar{k} = 0$ and assuming $\mathbf{f} \in \left[L^2(\Omega)\right]^2$, we find that

8

$$|\langle \mathbf{f}_h, \mathbf{v}_h \rangle - (\mathbf{f}, \mathbf{v}_h)| = \left| \sum_{E \in \Omega_h} \int_E \left(\Pi_0^{0,E} \mathbf{f} - \mathbf{f} \right) \mathbf{v}_h \, d\mathbf{x} \right| \leq \left| \sum_{E \in \Omega_h} \int_E \left(\Pi_0^{0,E} \mathbf{f} - \mathbf{f} \right) \left(\mathbf{v}_h - \Pi_0^{0,E} \mathbf{v}_h \right) d\mathbf{x} \right|$$

$$\leq \sum_{E \in \Omega_h} ||\Pi_{\overline{k}}^{0,E} \mathbf{f} - \mathbf{f}||_{0,E} \, ||\mathbf{v}_h - \Pi_0^{0,E} \mathbf{v}_h||_{0,E} \leq C h ||\mathbf{f}||_{0,E} \, |\mathbf{v}_h|_{1,E}, \tag{33}$$

for some constant $C > 0$ independent of h.

4. Convergence theory in the energy norm

In this section, we present an abstract convergence result in the energy norm for the VEM based on the pair of finite dimensional functional spaces $\left(\mathbf{V}_k^h, Q_{k-1}^h \right)$, see Theorem 4.1. These result allows us to derive an estimate for the approximation error on the velocity and the pressure, see Corollary 4.2. To carry out the convergence analysis, we assume that the VEM using the pair $\left(\mathbf{V}_k^h, Q_{k-1}^h \right)$ is inf-sup stable on the mesh family that is used in the discretization. A proof of the inf-sup condition for $k \geq 2$ and the "non-enhanced" virtual element space $\mathbf{V}_k^h$ defined in (12) can be found in [9]. We also make use of the interpolants $\mathbf{v}_I$ and q_I, which are defined in all mesh elements as the virtual element vector-valued field in $\mathbf{V}_k^h$ and the scalar polynomial $q \in Q_{k-1}^h$ of two (smooth enough) vector-valued field $\mathbf{v}$ and scalar function q, respectively. An estimate of the interpolation error as well as of the projection error is reported in the final appendix.

Theorem 4.1 (Abstract convergence result) *Let* $(\mathbf{u}, p) \in \left[H_0^1(\Omega) \right]^2 \times L_0^2(\Omega)$ *denote the exact solution of the variational formulation of the Stokes problem given in (7)-(8). Let* $(\mathbf{u}_h, p_h) \in \mathbf{V}_k^h \times Q_{k-1}^h$ *denote the solution of the virtual element variational formulation* (9)-(10) *for any polynomial degree* $k \geq 1$ *on the mesh family* $\{\Omega_h\}_h$ *satisfying the mesh regularity assumptions (M1) − (M2). We also assume that the bilinear form* $b_h(\cdot, \cdot)$ *is* inf-sup stable *on the pair* $\mathbf{V}_k^h \times Q_{k-1}^h$, *i.e., a real positive constant* β *exists such taht*

$$\inf_{q_h \in Q_{k-1}^h \backslash \{0\}} \sup_{\mathbf{v}_h \in \mathbf{V}_k^h \backslash \{\mathbf{0}\}} \frac{b_h(\mathbf{v}_h, q_h)}{\|q_h\|_0 \, \|\mathbf{v}_h\|_0} \geq \beta > 0. \tag{34}$$

Then, the solution fields $(\mathbf{u}_h, p_h) \in \mathbf{V}_k^h \times Q_{k-1}^h$ *exist and are unique, and for every interpolation approximation* $\mathbf{u}_I \in \mathbf{V}_k^h$ *and piecewise polynomial approximation* $\mathbf{u}_\pi \in \left[\mathbb{P}_k(\Omega_h) \right]^2$, *the following abstract estimate holds:*

$$|\mathbf{u} - \mathbf{u}_h|_{1,\Omega} + ||p - p_h||_{0,\Omega} \leq C \left(|\mathbf{u} - \mathbf{u}_I|_{1,\Omega} + |\mathbf{u} - \mathbf{u}_\pi|_{1,h} + ||p - p_I||_{0,\Omega} + \sup_{\mathbf{v}_h \in \mathbf{V}_k^h \backslash \{0\}} \frac{|\langle \mathbf{f}_h, \mathbf{v}_h \rangle - (\mathbf{f}, \mathbf{v}_h)|}{|\mathbf{v}_h|_{1,\Omega}} \right) \tag{35}$$

for some real, strictly positive constant C *independent of* h.

Proof. First, we note that the stability property (23) and the Cauchy-Schwarz inequality imply that

$$|a_h(\mathbf{v}_h, \mathbf{w}_h)| \leq C |\mathbf{v}_h|_{1,\Omega} \, |\mathbf{w}_h|_{1,\Omega} \qquad \forall \mathbf{v}_h, \, \mathbf{w}_h \in \mathbf{V}_k^h, \tag{36}$$

$$C |\mathbf{v}_h|_{1,\Omega}^2 \leq a_h(\mathbf{v}_h, \mathbf{v}_h) \qquad \forall \mathbf{v}_h \in \mathbf{V}_k^h, \tag{37}$$

for some real, strictly positive constant C. The bilinear form $b_h(\cdot, \cdot)$ is bounded since an application of the Cauchy-Schwarz inequality yields that

$$|b_h(\mathbf{v}_h, q)| \leq C |\mathbf{v}_h|_{1,\Omega} \, ||q||_{0,\Omega} \qquad \forall \mathbf{v}_h \in \mathbf{V}_k^h, \, q \in \mathbb{P}_{k-1}(\Omega_h).$$

The wellposedness of the VEM follows from the coercivity and boundedness of the bilinear form $a_h(\cdot, \cdot)$ and the boundedness and the inf-stability of the bilinear form $b_h(\cdot, \cdot)$ (the latter assumed in the theorem statement) [37].

To prove inequality (35), we introduce the virtual element field $\boldsymbol{\delta}_h = \mathbf{u}_h - \mathbf{u}_I \in \mathbf{V}_k^h$. The coercivity of $a_h(\cdot, \cdot)$, cf. Eq. (37), implies that:

$$C |\boldsymbol{\delta}_h|_{1,\Omega}^2 \leq a_h(\boldsymbol{\delta}_h, \boldsymbol{\delta}_h) = a_h(\mathbf{u}_h, \boldsymbol{\delta}_h) - a_h(\mathbf{u}_I, \boldsymbol{\delta}_h).$$

9

Then, we use (9) and we add and substract $\mathbf{u}_\pi$, we use (A.5) and (24), and add and substract $\mathbf{u}$ to obtain:

$$C|\boldsymbol{\delta}_h|_{1,\Omega}^2 \leq \langle \mathbf{f}_h, \boldsymbol{\delta}_h \rangle - b_h(\boldsymbol{\delta}_h, p_h) - \sum_{E \in \Omega_h} \left(a_h^E(\mathbf{u}_I - \mathbf{u}_\pi, \boldsymbol{\delta}_h) + a_h^E(\mathbf{u}_\pi, \boldsymbol{\delta}_h) \right)$$

$$= \langle \mathbf{f}_h, \boldsymbol{\delta}_h \rangle - b_h(\boldsymbol{\delta}_h, p_I) - \sum_{E \in \Omega_h} \left(a_h^E(\mathbf{u}_I - \mathbf{u}_\pi, \boldsymbol{\delta}_h) + a^E(\mathbf{u}_\pi, \boldsymbol{\delta}_h) \right)$$

$$= \langle \mathbf{f}_h, \boldsymbol{\delta}_h \rangle - b_h(\boldsymbol{\delta}_h, p_I) - \sum_{E \in \Omega_h} a_h^E(\mathbf{u}_I - \mathbf{u}_\pi, \boldsymbol{\delta}_h)$$

$$- \sum_{E \in \Omega_h} \left(a^E(\mathbf{u}_\pi - \mathbf{u}, \boldsymbol{\delta}_h) + a^E(\mathbf{u}, \boldsymbol{\delta}_h) \right)$$

We use (19), (7), and rearrange the terms:

$$C|\boldsymbol{\delta}_h|_{1,\Omega}^2 \leq \langle \mathbf{f}_h, \boldsymbol{\delta}_h \rangle - b_h(\boldsymbol{\delta}_h, p_I) - \sum_{E \in \Omega_h} a_h^E(\mathbf{u}_I - \mathbf{u}_\pi, \boldsymbol{\delta}_h) - \sum_{E \in \Omega_h} a^E(\mathbf{u}_\pi - \mathbf{u}, \boldsymbol{\delta}_h)$$

$$- a(\mathbf{u}, \boldsymbol{\delta}_h)$$

$$= \langle \mathbf{f}_h, \boldsymbol{\delta}_h \rangle - b_h(\boldsymbol{\delta}_h, p_I) - \sum_{E \in \Omega_h} a_h^E(\mathbf{u}_I - \mathbf{u}_\pi, \boldsymbol{\delta}_h) - \sum_{E \in \Omega_h} a^E(\mathbf{u}_\pi - \mathbf{u}, \boldsymbol{\delta}_h)$$

$$- \left((\mathbf{f}, \boldsymbol{\delta}_h) - b(\boldsymbol{\delta}_h, p) \right)$$

$$= \left[\langle \mathbf{f}_h, \boldsymbol{\delta}_h \rangle - (\mathbf{f}, \boldsymbol{\delta}_h) \right] + \left[b(\boldsymbol{\delta}_h, p_I) - b_h(\boldsymbol{\delta}_h, p) \right]$$

$$+ \left[- \sum_{E \in \Omega_h} a_h^E(\mathbf{u}_I - \mathbf{u}_\pi, \boldsymbol{\delta}_h) - \sum_{E \in \Omega_h} a^E(\mathbf{u}_\pi - \mathbf{u}, \boldsymbol{\delta}_h) \right]$$

$$= \left[(\mathbf{R1}) \right] + \left[(\mathbf{R2}) \right] + \left[(\mathbf{R3}) \right].$$

At this point, we continue estimating separately the three terms $(\mathbf{R1})$, $(\mathbf{R2})$, and $(\mathbf{R3})$, which are identified in the last step of the above inequality chain by the square brackets.

Term $(\mathbf{R1})$ is bounded from above by multiplying and dividing by $\boldsymbol{\delta}_h$, and then taking the supremum

$$\left| (\mathbf{R1}) \right| = |\langle \mathbf{f}_h, \boldsymbol{\delta}_h \rangle - (\mathbf{f}, \boldsymbol{\delta}_h)| = \frac{|\langle \mathbf{f}_h, \boldsymbol{\delta}_h \rangle - (\mathbf{f}, \boldsymbol{\delta}_h)|}{|\boldsymbol{\delta}_h|_{1,\Omega}} |\boldsymbol{\delta}_h|_{1,\Omega}$$

$$\leq \left[\sup_{\mathbf{v}_h \in \mathbf{V}_k^h} \frac{|\langle \mathbf{f}_h, \mathbf{v}_h \rangle - (\mathbf{f}, \mathbf{v}_h)|}{|\mathbf{v}_h|_{1,\Omega}} \right] |\boldsymbol{\delta}_h|_{1,\Omega}.$$

Term $(\mathbf{R2})$ is bounded from above by noting that $b_h^E(\mathbf{v}_h, p_I) = b^E(\mathbf{v}_h, p_I)$ in view of the definition of $b_h^E(\cdot, \cdot)$ and the orthogonal projection operator $\Pi_{k-1}^{0,E}$, cf. Equation (29). Summing over all the elements yields the identity $b_h(\mathbf{v}_h, p_I) = b(\mathbf{v}_h, p_I)$, and on applying such identity and the Cauchy-Schwarz inequality, we find that

$$\left| (\mathbf{R2}) \right| = |b(\boldsymbol{\delta}_h, p) - b_h(\boldsymbol{\delta}_h, p_I)| = |b(\boldsymbol{\delta}_h, p - p_I)| \leq ||\mathrm{div}\, \boldsymbol{\delta}_h||_{0,\Omega} ||p - p_I||_{0,\Omega}$$

$$\leq |\boldsymbol{\delta}_h|_{1,\Omega} ||p - p_I||_{0,\Omega}$$

Finally, term $(\mathbf{R3})$ is bounded from above by first using the continuity of $a_h(\cdot, \cdot)$, cf. (26), and of $a(\cdot, \cdot)$, the stability property (23)

10

$$\left|(\mathbf{R3})\right| = \left|\sum_{E\in\Omega_h} \left(a_h^E(\mathbf{u}_I - \mathbf{u}_\pi, \boldsymbol{\delta}_h) + a^E(\mathbf{u}_\pi - \mathbf{u}, \boldsymbol{\delta}_h)\right)\right|$$

$$\leq \sum_{E\in\Omega_h} \left(\left|a_h^E(\mathbf{u}_I - \mathbf{u}, \boldsymbol{\delta}_h)\right| + \left|a_h^E(\mathbf{u} - \mathbf{u}_\pi, \boldsymbol{\delta}_h)\right| + \left|a^E(\mathbf{u}_\pi - \mathbf{u}, \boldsymbol{\delta}_h)\right|\right)$$

Then, we add and subtract $\mathbf{u}$ in the first summation argument, and, in the last step, we introduce the broken seminorm $|\cdot|_{1,h}^2 = \sum_{E\in\Omega_h}|\cdot|_{1,E}^2$ to find that

$$\left|(\mathbf{R3})\right| \leq \alpha^* \sum_{E\in\Omega_h} \left(|\mathbf{u}_I - \mathbf{u}|_{1,E} + |\mathbf{u} - \mathbf{u}_\pi|_{1,E} + |\mathbf{u} - \mathbf{u}_\pi|_{1,E}\right) |\boldsymbol{\delta}_h|_{1,E}$$

$$\leq \left(\alpha^*|\mathbf{u} - \mathbf{u}_I|_{1,\Omega} + (1+\alpha^*)|\mathbf{u} - \mathbf{u}_\pi|_{1,h}\right) |\boldsymbol{\delta}_h|_{1,\Omega}.$$

We are left to derive a bound for the pressure term. To this end, we consider $\sigma_h = p_h - p_I$. Note that p_h is the solution of (9)-(10) and its cell average is zero on Ω as

$$\int_\Omega p_I \, d\mathbf{x} = \int_\Omega p \, d\mathbf{x} = 0.$$

We start the derivation of a bound for $||\sigma_h||_{0,\Omega}$ from the inf-sup condition (34). Then, we split $\sigma_h = p_h - p_I$, and use equations (9) and (7)

$$\beta||\sigma_h||_{0,\Omega}|\mathbf{v}_h|_{1,\Omega} \leq b_h(\mathbf{v}_h, \sigma_h) = b_h(\mathbf{v}_h, p_h) - b_h(\mathbf{v}_h, p_I)$$

$$= -a_h(\mathbf{u}_h, \mathbf{v}_h) + \langle\mathbf{f}_h, \mathbf{v}_h\rangle - b_h(\mathbf{v}_h, p_I)$$

$$= -a_h(\mathbf{u}_h, \mathbf{v}_h) + a(\mathbf{u}, \mathbf{v}_h) + b(\mathbf{v}_h, p) - (\mathbf{f}, \mathbf{v}_h)$$

$$+ \langle\mathbf{f}_h, \mathbf{v}_h\rangle - b_h(\mathbf{v}_h, p_I)$$

Then, we use (19) and (21), use (24) with $\mathbf{p} = \mathbf{u}_\pi$ and find that

$$\beta||\sigma_h||_{0,\Omega}|\mathbf{v}_h|_{1,\Omega} \leq \sum_{E\in\Omega_h} \left(a^E(\mathbf{u}, \mathbf{v}_h) - a_h^E(\mathbf{u}_h, \mathbf{v}_h)\right) + \langle\mathbf{f}_h, \mathbf{v}_h\rangle - (\mathbf{f}, \mathbf{v}_h)$$

$$+ b(\mathbf{v}_h, p) - b_h(\mathbf{v}_h, p_I)$$

$$= \sum_{E\in\Omega_h} \left(a^E(\mathbf{u} - \mathbf{u}_\pi, \mathbf{v}_h) - a_h^E(\mathbf{u}_h - \mathbf{u}_\pi, \mathbf{v}_h)\right) + \left[\langle\mathbf{f}_h, \mathbf{v}_h\rangle - (\mathbf{f}, \mathbf{v}_h)\right]$$

$$+ \left[b(\mathbf{v}_h, p) - b_h(\mathbf{v}_h, p_I)\right]$$

$$= \left[(\mathbf{R4})\right] + \left[(\mathbf{R5})\right] + \left[(\mathbf{R6})\right], \tag{38}$$

where, again, terms $(\mathbf{R4})$, $(\mathbf{R5})$, and $(\mathbf{R6})$ are identified by the square brackets. As for the term $\boldsymbol{\delta}_h$, we continue estimating each term separately.

Term $(\mathbf{R4})$ is bounded from above as we bounded term $(\mathbf{R3})$, only using $\mathbf{v}_h$ instead of $\boldsymbol{\delta}_h$ to to find that:

$$\left|(\mathbf{R4})\right| \leq \alpha^* \left(|\mathbf{u} - \mathbf{u}_I|_{1,\Omega} + 2|\mathbf{u} - \mathbf{u}_\pi|_{1,h}\right) |\mathbf{v}_h|_{1,\Omega},$$

Term $(\mathbf{R5})$ is bounded from above as we bounded term $(\mathbf{R1})$, just using again $\mathbf{v}_h$ instead of $\boldsymbol{\delta}_h$

$$\left|(\mathbf{R5})\right| = |\langle\mathbf{f}_h, \mathbf{v}_h\rangle - (\mathbf{f}, \mathbf{v}_h)| \leq \left[\sup_{\mathbf{v}_h\in\mathbf{V}_k^h} \frac{|\langle\mathbf{f}_h, \mathbf{v}_h\rangle - (\mathbf{f}, \mathbf{v}_h)|}{|\mathbf{v}_h|_{1,\Omega}}\right] |\mathbf{v}_h|_{1,\Omega}.$$

Finally, term $(\mathbf{R6})$ is bounded as we bounded $(\mathbf{R2})$, just $\mathbf{v}_h$ instead of $\boldsymbol{\delta}_h$ for the last time

$$\left|(\mathbf{R6})\right| \leq |\mathbf{v}_h|_{1,\Omega} \, ||p_I - p||_{0,\Omega}.$$

11

Eventually, we obtain the energy estimate of inequality (35) by adding and substracting $\mathbf{u}_I$ and p_I in the two terms of the left-hand side of (35) and using the triangle inequality:

$$|\mathbf{u} - \mathbf{u}_h|_{1,\Omega} \leq |\mathbf{u} - \mathbf{u}_I|_{1,\Omega} + |\mathbf{u}_I - \mathbf{u}_h|_{1,\Omega}, \tag{39}$$

$$||p - p_h||_{0,\Omega} \leq ||p - p_I||_{0,\Omega} + |p_I - p_h|_{0,\Omega}. \tag{40}$$

We estimate the first term in the right-hand side of the two inequalities above by using standard estimates of the interpolation errors provided by Lemma A.1 (see the appendix), and the second term by substituting the bounds we previously derived for the terms $(\mathbf{R1}) - (\mathbf{R6})$. □

An error estimate follows immediate from Theorem 4.1. We state it in the following corollary.

Corollary 4.2 (Error estimate) *Let* $(\mathbf{u}_h, p_h) \in \mathbf{V}_k^h \times Q_{k-1}^h$ *be the virtual element solution fields approximating* $\mathbf{u} \in \left[H^{s+1}(\Omega) \cap H_0^1(\Omega)\right]^2$ *and* $p \in H^s(\Omega) \cap L_0^2(\Omega)$, *and take* $\mathbf{f} \in \left[H^s(\Omega)\right]^2$ *for* $1 \leq s \leq k$. *Then, under assumption of Theorem 4.1, it holds that*

$$|\mathbf{u} - \mathbf{u}_h|_{1,\Omega} + ||p - p_h||_{0,\Omega} \leq Ch^s \left(||\mathbf{u}||_{s+1,\Omega} + ||p||_{s,\Omega} + ||\mathbf{f}||_{s,\Omega}\right) \tag{41}$$

for some real, strictly positive constant C *independent of* h.

Proof. Finally, estimate (41) follows from a straightforward application of the results of Lemmas A.2 and A.1, and estimates (32)-(33) to the right-hand side of (35). □

5. Numerical experiments

We assess the convergence property of the virtual element method proposed in this paper by numerically solving problem (7)-(8) on the computational domain $\Omega = [0,1] \times [0,1]$, which we partition using the grids of the six mesh families $\mathcal{M}1$, $\mathcal{M}2$, and $\mathcal{M}3$ of Figure 2 and $\mathcal{M}4$, $\mathcal{M}5$, and $\mathcal{M}6$ of Figure 3. Table 1 reports the diameters of every mesh for the six mesh families and all refinement levels. Tables 2 and 3 report the number of elements and vertices for the mesh families $\mathcal{M}1$-$\mathcal{M}3$ and $\mathcal{M}4$-$\mathcal{M}6$, respectively.

Dirichlet boundary conditions and source terms are set accordingly to the manufactured solution $\mathbf{u} = (u_x, u_y)^T$ and p given by

$$u_x(x, y) = \cos(2\pi x)\sin(2\pi y),$$
$$u_y(x, y) = -\sin(2\pi x)\cos(2\pi y),$$
$$p(x, y) = e^{x+y} - (e-1)^2.$$

On any set of refined meshes, we measure the H^1 relative error for the velocity vector field by applying the formula

$$\text{error}_{H^1(\Omega)}(\mathbf{u}) = \frac{|\mathbf{u} - \Pi_k^0 \mathbf{u}_h|_{1,h}}{|\mathbf{u}|_{1,\Omega}} \approx \frac{|\mathbf{u} - \mathbf{u}_h|_{1,\Omega}}{|\mathbf{u}|_{1,\Omega}}, \tag{42}$$

and the L^2 relative error by applying the formula

$$\text{error}_{L^2(\Omega)}(\mathbf{u}) = \frac{||\mathbf{u} - \Pi_k^0 \mathbf{u}_h||_{0,\Omega}}{||\mathbf{u}||_{0,\Omega}} \approx \frac{||\mathbf{u} - \mathbf{u}_h||_{0,\Omega}}{||\mathbf{u}||_{0,\Omega}}, \tag{43}$$

where $\left(\Pi_k^0 \mathbf{u}_h\right)_{|E} = \Pi_k^{0,E}(\mathbf{u}_{h|E})$. For the pressure scalar field we measure the $L^2(\Omega)$ relative error by applying the formula

$$\text{error}_{L^2(\Omega)}(p) = \frac{||p - p_h||_{0,\Omega}}{||p||_{0,\Omega}}. \tag{44}$$

The discretization of the bilinear form $a_h(\cdot, \cdot)$ and $b_h(\cdot, \cdot)$ yields two matrices A and B, respectively, while the discretization of the right-hand side gives the vector $\underline{\mathbf{f}}_h$.

To write the formal expression of such matrices we introduce the canonical shape functions Φ_j of the virtual element space $\mathbf{V}_k^h(E)$, and the basis functions $\mathbf{m}_\alpha$ of the local polynomial space $\left[\mathbb{P}_\ell(E)\right]^2$, where ℓ can be equal to $k-1$ or k. We can assume that space $\mathbb{P}_\ell(E)$ is the span of the finite set of *scaled monomials of degree up to* ℓ, that are given by
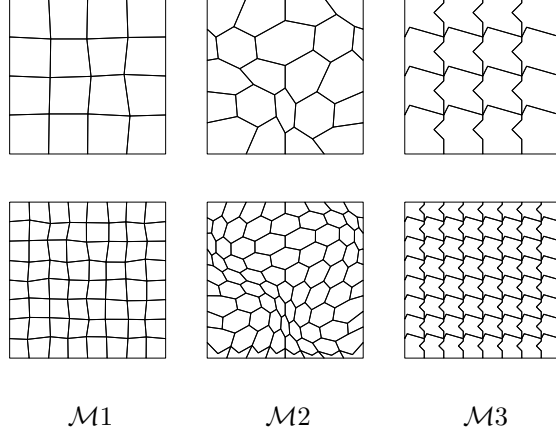
Fig. 2. Base meshes (top row) and first refinement meshes (bottom row) of the three mesh families used in the general convergence tests: $\mathcal{M}1$: randomly quadrilateral meshes; $\mathcal{M}2$: general polygonal meshes; $\mathcal{M}3$: concave element meshes;
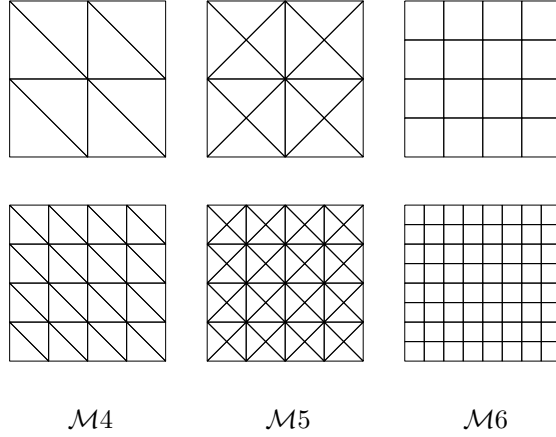

Fig. 3. Base meshes (top row) and first refinement meshes (bottom row) of the three mesh families used to investigate convergence and stability of the lowest-order scheme: $\mathcal{M}4$: diagonal triangle meshes; $\mathcal{M}5$: criss-cross triangle meshes; $\mathcal{M}6$: square meshes.

Level	$\mathcal{M}1$	$\mathcal{M}2$	$\mathcal{M}3$	$\mathcal{M}4$	$\mathcal{M}5$	$\mathcal{M}6$
1	$3.72 \cdot 10^{-1}$	$4.26 \cdot 10^{-1}$	$3.81 \cdot 10^{-1}$	$7.07 \cdot 10^{-1}$	$5.00 \cdot 10^{-1}$	$3.53 \cdot 10^{-1}$
2	$1.99 \cdot 10^{-1}$	$2.50 \cdot 10^{-1}$	$1.91 \cdot 10^{-1}$	$3.53 \cdot 10^{-1}$	$2.50 \cdot 10^{-1}$	$1.77 \cdot 10^{-1}$
3	$1.01 \cdot 10^{-1}$	$1.25 \cdot 10^{-1}$	$9.54 \cdot 10^{-2}$	$1.77 \cdot 10^{-1}$	$1.25 \cdot 10^{-1}$	$8.84 \cdot 10^{-2}$
4	$5.17 \cdot 10^{-2}$	$6.21 \cdot 10^{-2}$	$4.77 \cdot 10^{-2}$	$8.84 \cdot 10^{-2}$	$6.25 \cdot 10^{-1}$	$4.42 \cdot 10^{-2}$
5	$2.61 \cdot 10^{-2}$	$3.41 \cdot 10^{-2}$	$2.38 \cdot 10^{-2}$	$4.42 \cdot 10^{-2}$	$3.12 \cdot 10^{-2}$	$2.21 \cdot 10^{-2}$

Table 1
Diameter h of each grid of the six mesh families $\mathcal{M}1$-$\mathcal{M}6$.

$$\mathcal{M}_\ell(E) = \left\{ \left(\frac{\mathbf{x} - \mathbf{x}_E}{h_E} \right)^\alpha \text{ with } |\alpha| \leq \ell \right\},$$

where
- $\mathbf{x}_E$ denotes the center of gravity of E and h_E its characteristic length, e.g., the cell diameter;
- $\alpha = (\alpha_1, \alpha_2)$ is the two-dimensional multi-index of nonnegative integers α_i with degree $|\alpha| = \alpha_1 + \alpha_2 \leq \ell$ and such that $\mathbf{x}^\alpha = x_1^{\alpha_1} x_2^{\alpha_2}$ for any $\mathbf{x} \in \mathbb{R}^2$ and $\partial^{|\alpha|}/\partial\mathbf{x}^\alpha = \partial^{|\alpha|}/\partial x_1^{\alpha_1} \partial x_2^{\alpha_2}$.

Alternatively, we can assume that space $\mathbb{P}_\ell(E)$ is the span of a set of orthogonalized polynomials built from the scaled monomials by applying the Gram-Schmidt process in all elements E, see [65].

Now, the entries of the global matrix A are given by assembling the local consistency and stability matrices,

Level	$\mathcal{M}1$		$\mathcal{M}2$		$\mathcal{M}3$	
	N_{el}	N	N_{el}	N	N_{el}	N
1	16	25	22	46	16	73
2	64	81	84	171	64	305
3	256	289	312	628	256	1249
4	1024	1089	1202	2406	1024	5057
5	4096	4225	4772	9547	4096	20353

Table 2
Number of elements N_{el} and vertices N of each grid of the three mesh families $\mathcal{M}1$–$\mathcal{M}3$.

Level	$\mathcal{M}4$		$\mathcal{M}5$		$\mathcal{M}6$	
	N_{el}	N	N_{el}	N	N_{el}	N
1	8	9	16	13	16	25
2	32	25	64	41	64	81
3	128	81	256	145	256	289
4	512	289	1024	545	1024	1089
5	2048	1089	4096	2113	4096	4225

Table 3
Number of elements N_{el} and vertices N of each grid of the three mesh families $\mathcal{M}4$–$\mathcal{M}6$.

$$\mathsf{A} = \sum_{\mathsf{E}} \mathsf{Q}^T \left(\mathsf{A}_{\mathsf{E}}^C + \mathsf{A}_{\mathsf{E}}^S \right) \mathsf{Q},$$

where Q is the assembling matrix that remaps the local entries of the elemental matrices $\mathsf{A}_{\mathsf{E}}^C$ and $\mathsf{A}_{\mathsf{E}}^S$ into the global setting of matrix A, and

$$(\mathsf{A}_{\mathsf{E}}^C)_{ij} = \int_{\mathsf{E}} \Pi_{k-1}^{0,\mathsf{E}} \nabla \Phi_i : \Pi_{k-1}^{0,\mathsf{E}} \nabla \Phi_j \, d\mathbf{x},$$

$$\mathsf{A}_{\mathsf{E}}^S = (I - \Pi^{\mathsf{E}})^T (I - \Pi^{\mathsf{E}}),$$

and Π^{E} is the matrix associated to the ortogonal projector $\Pi_k^{0,\mathsf{E}}$ or the elliptic projector $\Pi_k^{\nabla,\mathsf{E}}$ defined on the element E. Likewise, the global matrix B has entries given by assembling the local contributions of the integrals

$$(\mathsf{B}_{\mathsf{E}})_{\alpha j} = \int_{\mathsf{E}} m_\alpha \Pi_{\underline{k}}^{0,\mathsf{E}} \mathrm{div}\, \Phi_j \, d\mathbf{x}.$$

Denoting the vectors of the degrees of freedom of velocity and pressure by respectively $\underline{\mathbf{u}}_h$ and $\underline{p}_h$, the problem to be solved reads as:

$$\begin{bmatrix} \mathsf{A} & \mathsf{B}^T \\ \mathsf{B} & 0 \end{bmatrix} \begin{bmatrix} \underline{\mathbf{u}}_h \\ \underline{p}_h \end{bmatrix} = \begin{bmatrix} \mathbf{f}_h \\ 0 \end{bmatrix} \tag{45}$$

To solve this system, we eliminate the degrees of freedom corresponding to the Dirichlet conditions, and impose the additional condition that $\int_\Omega p_h \, d\mathbf{x} = 0$ by introducing a Lagrange multiplier.

5.1. *General convergence results*

We compare the approximation errors (42), (43), and (44) obtained by applying the numerical scheme to the mesh families $\mathcal{M}1$, $\mathcal{M}2$, and $\mathcal{M}3$ and setting $\underline{k} = k - 1$. Figure 4 shows the approximation errors when the right-hand side is discretized by using the projection operator $\Pi_{\bar{k}}^{0,\mathsf{E}}$ with $\bar{k} = k$ for $k = 1, \ldots, 6$. This right-hand side definition requires the "enhanced" virtual element space (13). Figure 5 shows the approximation errors when the right-hand side is approximated by using the projection operator $\Pi_{\bar{k}}^{0,\mathsf{E}}$ with $\bar{k} = max(0, k-2)$. This right-hand side definition requires the "non-enhanced" virtual element space (12). When we set $\bar{k} = k$ we observe the optimal convergence rates in all the norms, so the error for the velocity in the energy norm and in the L^2-norm scales as $\mathcal{O}(h^k)$ and $\mathcal{O}(h^{k+1})$, respectively, and the error of the pressure scales as $\mathcal{O}(h^k)$, again for $k = 1, \ldots, 6$. When we set $\bar{k} = \max(0, k-2)$, we observe the optimal convergence rate for the velocity approximation for all $k \geq 1$ only in the energy norm. Instead, the velocity error in the L^2-norm looses an order of approximation when $k = 2$. Moreover, an overall better approximation, i.e., smaller errors, are visible when we select $\bar{k} = k$. Regarding the approximation of the zero-divergence constraint, in
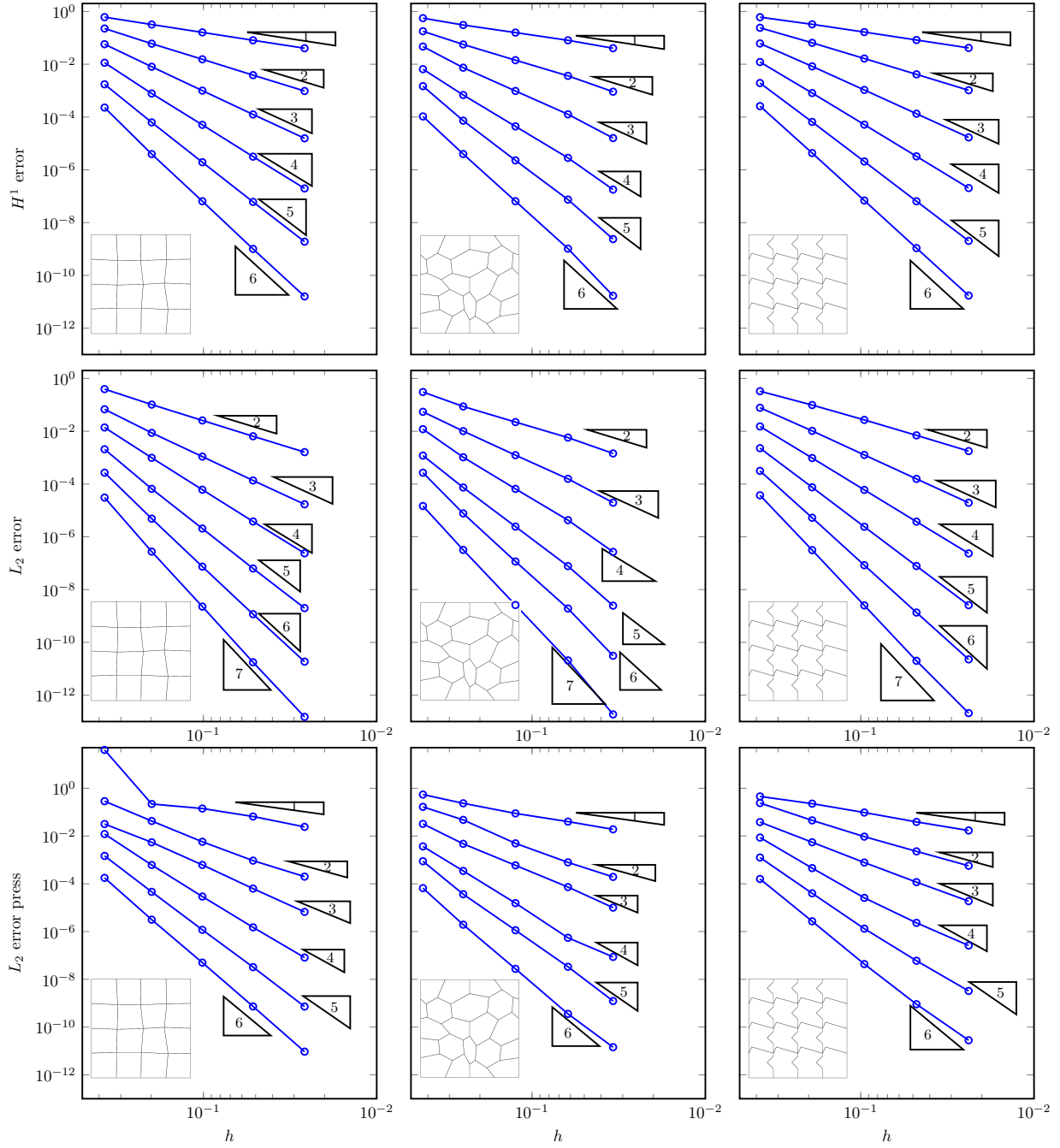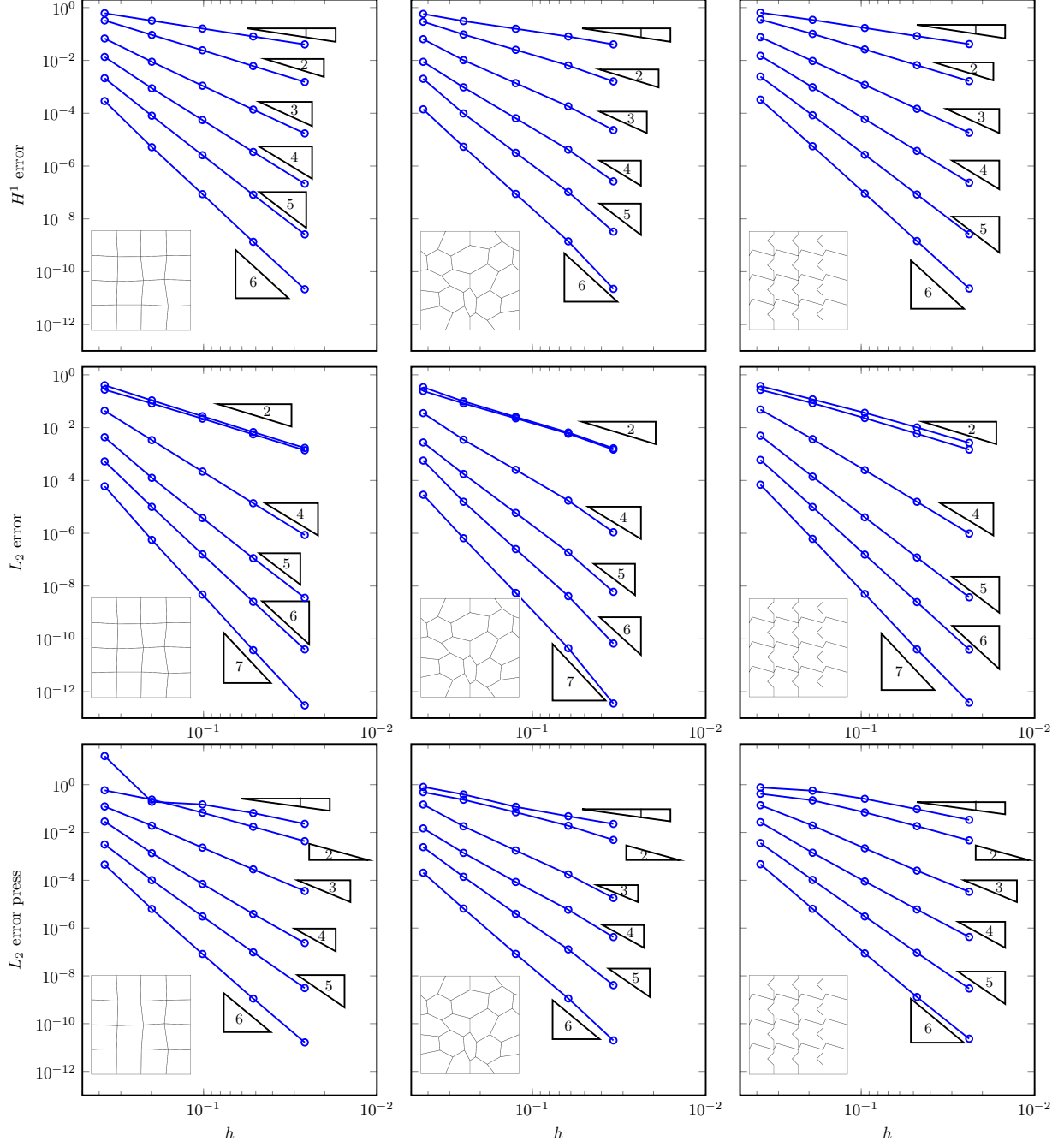
14

Fig. 4. Convergence curves for $k = 1, \ldots, 6$ and $\underline{k} = k - 1$ versus the mesh size parameter h for the velocity approximation measured using the energy norm (42) (top panels) and the L^2-norm (43) (mid panels), and for the pressure approximation measured using the L^2-norm (44) (bottom panels). Blue lines with circles represent the error curves using the enhanced virtual element space (13), and, accordingly, the right-hand is approximated by using the projection operator $\Pi_k^{0,E}$. The mesh families used in each calculations are shown in the left corner of each panel. The expected convergence slopes and rates are shown by the triangles and corresponding numerical labels.

all our experiments we noted that the divergence of the velocity is close to the machine precision. We do not report the plots of these results.

Fig. 5. Convergence curves for $k = 1, \ldots, 6$ and $\underline{k} = k - 1$ versus the mesh size parameter h for the velocity approximation measured using the energy norm (42) (top panels) and the L^2-norm (43) (mid panels), and for the pressure approximation measured using the L^2-norm (44) (bottom panels). Blue lines with circles represent the error curves using the virtual element space (12), and, accordingly, the right-hand is approximated by using the projection operator $\Pi_{\bar{k}}^{0,\mathrm{E}}$ with $\bar{k} = max(0, k - 2)$. A loss of accuracy for $k = 2$ in the L^2-norm error curves is visible. The mesh families used in each calculations are shown in the left corner of each panel. The expected convergence slopes and rates are shown by the triangles and corresponding numeric labels.

	$\mathcal{M}4$		
Level	size(B)	$rank(B)$	$kernel(B)$
1	2×8	2	6
2	18×32	18	14
3	98×128	98	30
4	450×512	450	62
5	1922×2048	1922	126
6	7938×8192	7938	254

Table 4

Size, rank and kernel's dimension of matrix B when $k = 1$ for the mesh family $\mathcal{M}4$.

	$\mathcal{M}5$		
Level	size(B)	$rank(B)$	$kernel(B)$
1	10×16	10	6
2	50×64	46	18
3	226×256	190	66
4	962×1024	766	258
5	3970×4096	3070	1026
6	16130×16384	12286	4098

Table 5

Size, rank and kernel's dimension of matrix B when $k = 1$ for the mesh family $\mathcal{M}5$.

5.2. *The lowest-order case for $k = 1$*

The case $k = 1$ is critical since on triangular and square meshes this scheme coincides with unstable schemes, as for example the $\mathbb{P}_1 - \mathbb{P}_0$ Scott-Vogelius method on triangular meshes. We experimentally investigate this issue by using the mesh families $\mathcal{M}4$, $\mathcal{M}5$ and $\mathcal{M}6$. Following [70] and using orthonormal polynomials, the relationship between the inf-sup constant β and the minimum non-zero eigenvalue of the matrix $\mathsf{BA}^{-1}\mathsf{B}^T$ is given by

$$\beta \simeq \sqrt{\lambda_{min}\big(\mathsf{BA}^{-1}\mathsf{B}^T\big)},$$

where λ_{min} is the smallest nonzero eigenvalue, and matrices B and A are so that (45) holds after removing the rows and columns that correspond to the boundary degrees of freedom. If l is the size of the kernel of matrix B, the rank of B is equal to $m = n_{\bar{k}} - l$, where $n_{\bar{k}}$ is the number of rows of B, and matrix $\mathsf{BA}^{-1}\mathsf{B}^T$ has size $n_{\bar{k}} \times n_{\bar{k}}$ and l eigenvalues equal to zero. If $l > 1$ matrix $\mathsf{BA}^{-1}\mathsf{B}^T$ is rank deficient (recall that constant vectors must always be in the kernel of B^T as this matrix "represents" a gradient, so ℓ must be at least 1), and the "inf-sup" condition cannot be satisfied for any positive number β.

In Figure 6, we show the values of the inf-sup constant β for $k = 1$ versus the mesh size parameter h of the diagonal, criss-cross and square meshes (we add a level of refinement in the meshes in order to see if and how β depends on h). It is evident from these plots that β approaches zero, revealing that the inf-sup condition is not satisfied.

Tables 4, 5 and 6 report size, rank and kernel's dimension of matrix B for the meshes $\mathcal{M}4$, $\mathcal{M}5$ and $\mathcal{M}6$ at the various refinement levels. We expect the kernel of B to be equal to 1 when the coefficient matrix of the global system (45) is nonsingular, i.e., when the inf-sup condition is satisfied and a value greater than 1 otherwise. For the triangular and criss-cross meshes the kernel of B is always greater than 1, with increasing values for increasing levels of the meshes, while for the square regular meshes the kernel is equal to 2 at all levels. This instability appears only when $k = 1$ and $\underline{k} = 0$. Indeed, Figure 7 shows the values of the inf-sup constant β for different pairs of integers $(k, \underline{k})$ and it is evident that β is constant for a decreasing h. We can also observe that the inf-sup condition is not satisfied on quadrilateral meshes only if regular squares are considered. Indeed, we directly checked that on the meshes of mesh family $\mathcal{M}1$, the kernel of B is always equal to 1.

Moreover, the numerical approximations obtained with $k \geq 2$ and $\underline{k} = k - 1$ give the expected results, as we can see from Figure 8.

5.3. *The case for $k = 2$ and $\underline{k} = 0$*

The results for the case $k = 2$, $\underline{k} = 0$ are shown in Figure 9. For the formulation with $k = 2$ for the velocity virtual element space and $\underline{k} = 0$ for the pressure, we observe that the velocity errors in the energy norm are very close when

17

Level	$\mathcal{M}6$		
	size(B)	$rank(B)$	$kernel(B)$
1	18×16	14	2
2	98×64	62	2
3	450×256	254	2
4	1922×1024	1022	2
5	7938×4096	4094	2
6	32258×16384	16382	2

Table 6
Size, rank and kernel's dimension of matrix B when $k = 1$ for the mesh family $\mathcal{M}6$.
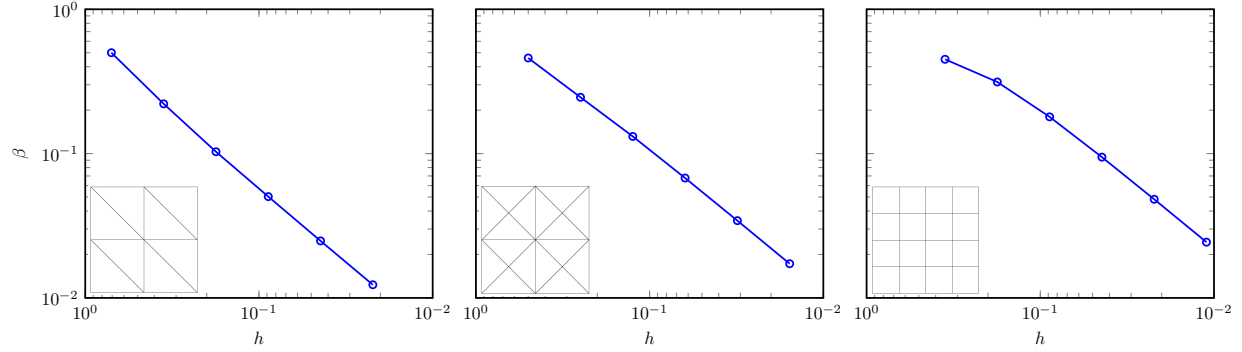
Fig. 6. Values of the inf-sup constant β versus the mesh size parameter h. The lines with circles represent the values of β with $k = 1$ and $\underline{k} = 0$. The mesh families used in each calculations are shown in the bottom-left corner of each panel.
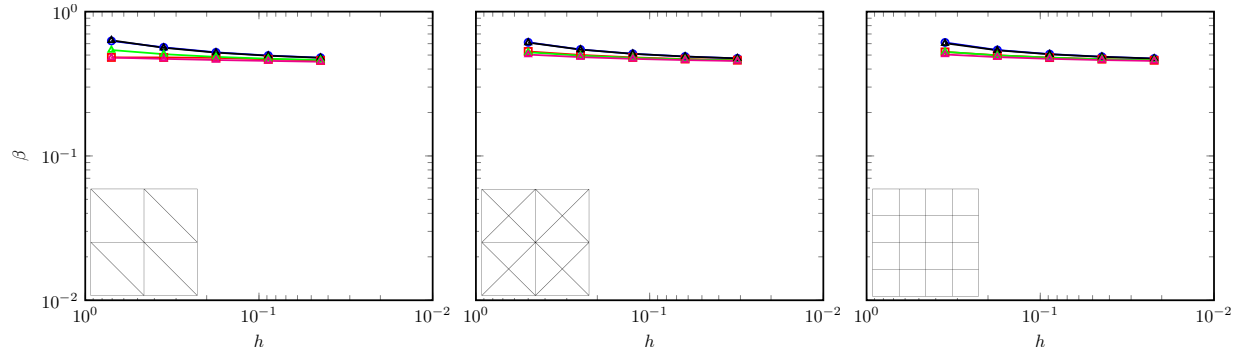
Fig. 7. Values of the inf-sup constant β versus the mesh size parameter h. Blue lines with circles represent the values of β with $k = 2$ and $\underline{k} = 0$. Red lines with circles represent the values of β when $k = 2$ and $\underline{k} = 1$. Black, green and magenta lines with triangles are associate to $k = 3$ and $\underline{k} = 0$, $\underline{k} = 1$ and $\underline{k} = 2$, respectively. The mesh families used in each calculations are shown in the bottom-left corner of each panel.

we use the projection $\Pi_0^{0,\mathrm{E}}$ or the projection $\Pi_2^{0,\mathrm{E}}$ in the discretization of the right-hand side. In both cases we obtain the expected rate of convergence of order 2. On the contrary, if we measure the error using the L^2-norm, we note a convergence of order between 2 and 3 when the projector $\Pi_2^{0,\mathrm{E}}$ is applied, and a convergence of order 2 when the projector $\Pi_0^{0,\mathrm{E}}$ is applied.

For the approximation of the scalar unknown, the rate is approaching 1 in both cases and we observe better results with the Π_k^0 projector.

6. Conclusions

We studied a conforming virtual element formulation that generalizes the Scott-Vogelius FEM for the numerical approximation of the Stokes problem to unstructured meshes and works at any order of accuracy. The components of the vector-valued unknown are approximated by using the conforming regular or enhanced virtual element approx-
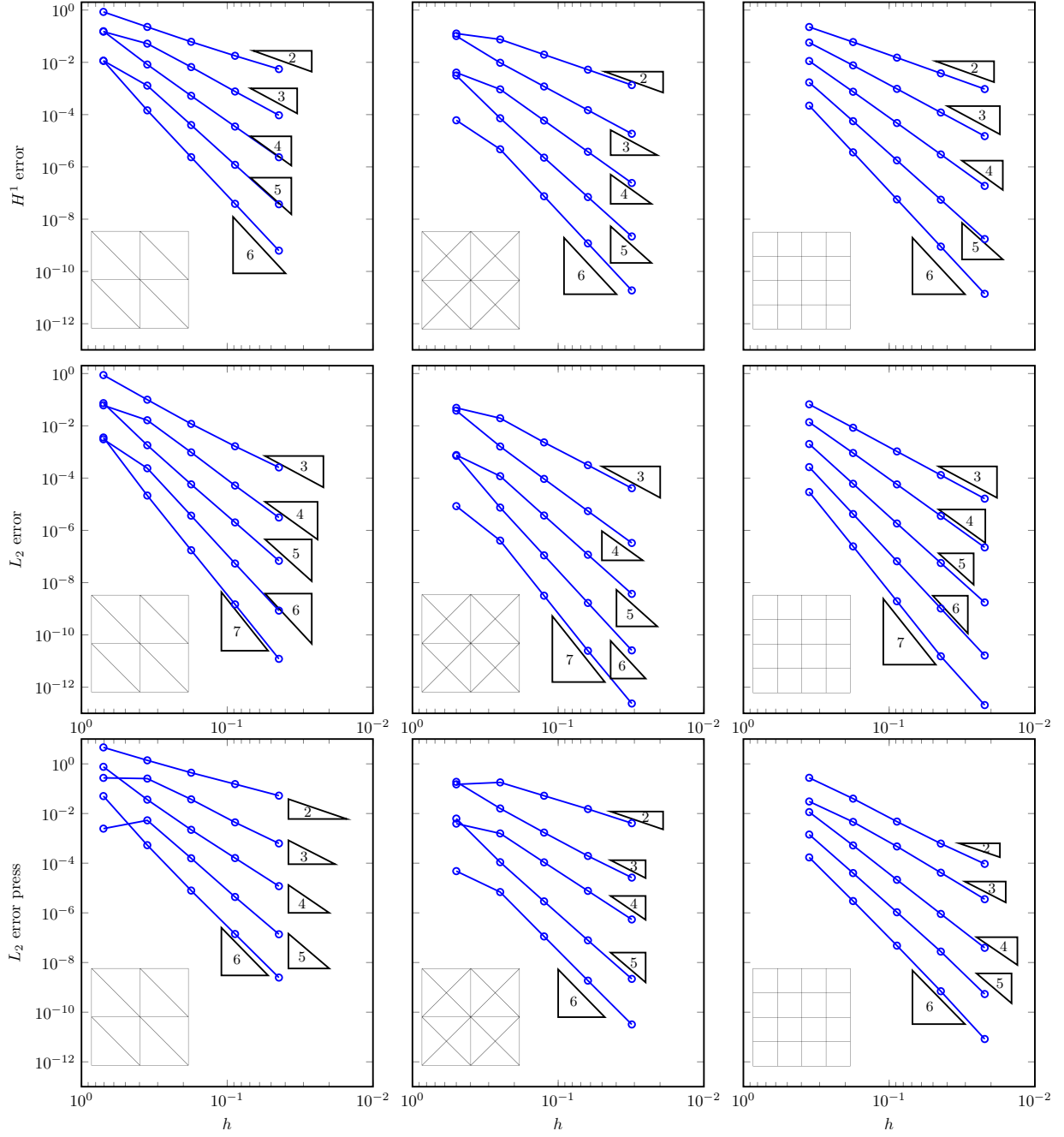
Fig. 8. Convergence curves for $k = 2, \ldots, 6$, and $\underline{k} = k - 1$ versus the mesh size parameter h for the velocity approximation measured using the energy norm (42) (top panels) and the L^2-norm (43) (mid panels), and for the pressure approximation measured using the L^2-norm (44) (bottom panels). The results with $k = 1$ are not reported because there is no convergence. The lines with circles represent the error curves using the enhanced virtual element space (13). The right-hand side is approximated by using the projection operator $\Pi_k^{0,E}$, i.e., the "enhanced" definition of the virtual element space given in (13). The mesh families used in each calculations are shown in the left corner of each panel. The expected convergence slopes and rates are shown by the triangles and corresponding numerical labels.
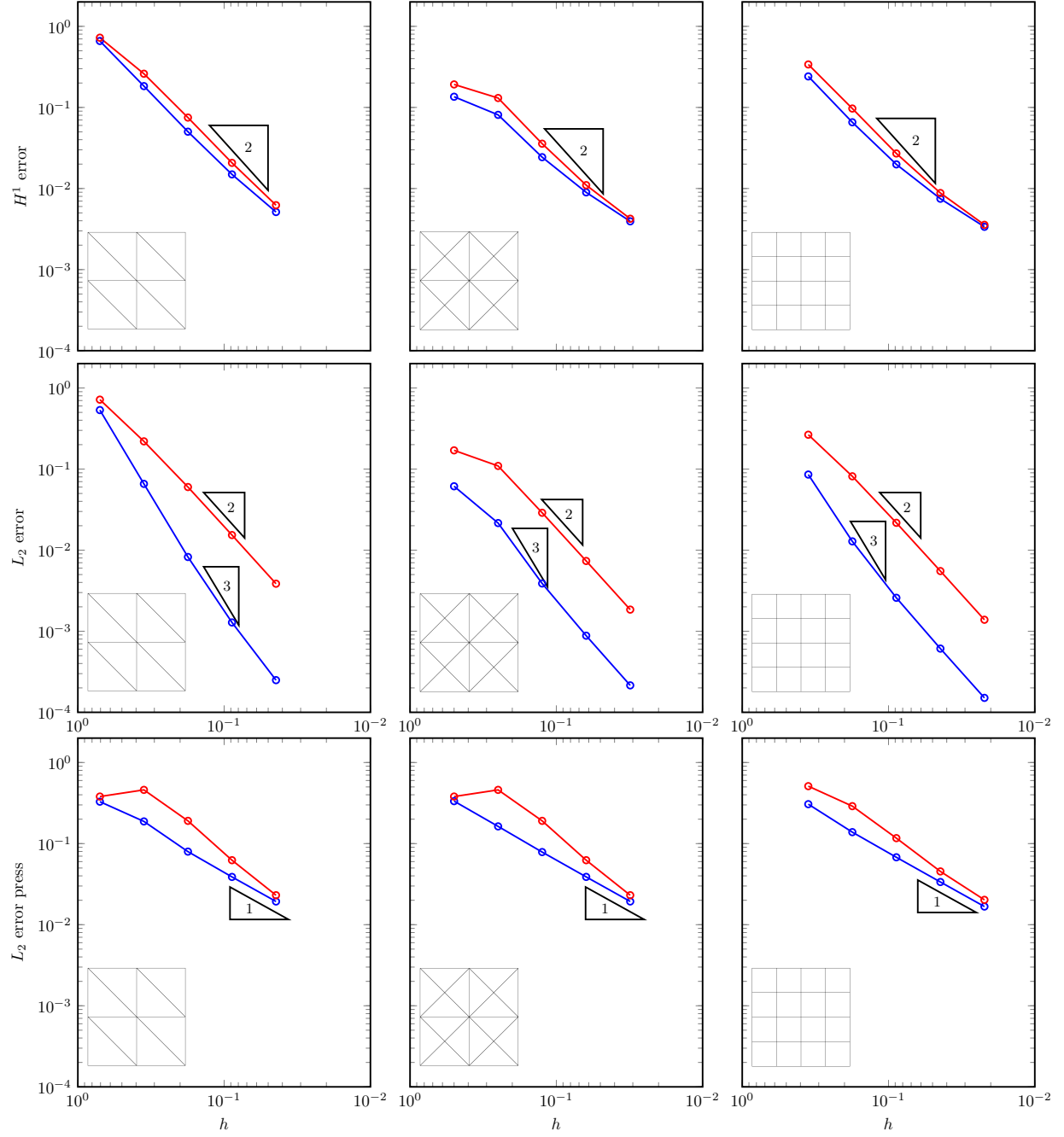
19

Fig. 9. Convergence curves for $k = 2$, $\underline{k} = 0$, versus the mesh size parameter h for the velocity approximation measured using the energy norm (42) (top panels) and the L^2-norm (43) (mid panels), and for the pressure approximation measured using the L^2-norm (44) (bottom panels). Blue lines with circles represent the error curves for the formulation using the enhanced virtual element space (13) with the right-hand side approximated by using the projection operator Π_2^0. Red lines with circles represent the error curve with the right-hand side approximated by using the projection operator Π_0^0. The mesh families used in each calculations are shown in the left corner of each panel. The convergence slopes and rates are shown by the triangles and corresponding numeric labels.

imation space that were originally introduced for the discretization of the Poisson equation. The scalar unknown is approximated by using discontinuous polynomials. The stiffness bilinear form is approximated by using the orthogonal polynomial projection of the gradients onto vector polynomials of degree $k - 1$ and adding a suitable stabilization term. The zero divergence constraint is taken into account by projecting the divergence equation onto the space of polynomials of degree $k - 1$. We presented a number of numerical experiments to demonstrate that this formulation is inf-sup stable and convergent with optimal convergence rates except for the lowest-order case (e.g., for the polynomial order $k = 1$) on triangular meshes, which corresponds to the well-known $\mathbb{P}_1 - \mathbb{P}_0$ unstable method of the Scott-Vogelius method, and squares meshes. Moreover, our numerical experiments show that the divergence constraint is satisfied at the machine precision level by the orthogonal polynomial projection of the divergence of the approximate velocity vector.

Acknowledgments

References

[1] R. A. Adams and J. J. F. Fournier. *Sobolev spaces*. Pure and Applied Mathematics. Academic Press, 2 edition, 2003.

[2] B. Ahmad, A. Alsaedi, F. Brezzi, L. D. Marini, and A. Russo. Equivalent projectors for virtual element methods. *Comput. Math. Appl.*, 66:376–391, September 2013.

[3] P. F. Antonietti, L. Beirão da Veiga, D. Mora, and M. Verani. A stream virtual element formulation of the Stokes problem on polygonal meshes. *SIAM J. Numer. Anal.*, 52(1):386–404, 2014.

[4] P. F. Antonietti, G. Manzini, and M. Verani. The fully nonconforming Virtual Element method for biharmonic problems. *Math. Models Methods Appl. Sci.*, 28(2), 2018.

[5] P. F. Antonietti, G. Manzini, and M. Verani. The conforming virtual element method for polyharmonic problems. *Comput. Math. Appl.*, 79(7):2021–2034, 2020. published online: 4 October 2019.

[6] B. Ayuso de Dios, K. Lipnikov, and G. Manzini. The non-conforming virtual element method. *ESAIM Math. Model. Numer.*, 50(3):879–904, 2016.

[7] B. Bang and D. Lukkassen. Application of homogenization theory related to Stokes flow in porous media. *Applications of Mathematics*, 44:309–319, 1999.

[8] L. Beirão da Veiga, F. Brezzi, A. Cangiani, G. Manzini, L. D. Marini, and A. Russo. Basic principles of virtual element methods. *Math. Models Methods Appl. Sci.*, 23:119–214, 2013.

[9] L. Beirão da Veiga, F. Brezzi, and L. D. Marini. Virtual elements for linear elasticity problems. *SIAM J. Numer. Anal.*, 51(2):794–812, 2013.

[10] L. Beirão da Veiga, F. Brezzi, L. D. Marini, and A. Russo. The hitchhiker's guide to the virtual element method. *Math. Models Methods Appl. Sci*, 24(8):1541–1573, 2014.

[11] L. Beirão da Veiga, F. Brezzi, L. D. Marini, and A. Russo. Virtual element methods for general second order elliptic problems on polygonal meshes. *Math. Models Methods Appl. Sci.*, 26(04):729–750, 2015.

[12] L. Beirão da Veiga, F. Brezzi, L. D. Marini, and A. Russo. H(div) and H(curl)-conforming VEM. *Numer. Math.*, 133(2):303–332, 2016.

[13] L. Beirão da Veiga, F. Brezzi, L. D. Marini, and A. Russo. Mixed virtual element methods for general second order elliptic problems on polygonal meshes. *ESAIM Math. Model. Num.*, 50(3):727–747, 2016.

[14] L. Beirão da Veiga, F. Brezzi, L. D. Marini, and A. Russo. Serendipity nodal VEM spaces. *Computers and Fluids*, 141:2–12, 2016.

[15] L. Beirão da Veiga, F. Brezzi, L. D. Marini, and A. Russo. Virtual element methods for general second order elliptic problems on polygonal meshes. *Math. Models Methods Appl. Sci.*, 26(4):729–750, 2016.

[16] L. Beirão da Veiga, A. Chernov, L. Mascotto, and A. Russo. Basic principles of hp virtual elements on quasiuniform meshes. *Math. Models Methods Appl. Sci.*, 26(8):1567–1598, 2016.

[17] L. Beirão da Veiga, F. Dassi, and G. Vacca. The Stokes complex for virtual elements in three dimensions. *Math. Models Methods Appl. Sci.*, 30(03):477–512, 2020.

[18] L. Beirão da Veiga, V. Gyrya, K. Lipnikov, and G. Manzini. Mimetic finite difference method for the Stokes problem on polygonal meshes. *Journal of Computational Physics*, 228:7215–7232, 2009.

[19] L. Beirão da Veiga and K. Lipnikov. A mimetic discretization of the Stokes problem with selected edge bubbles. *SIAM J. Sci. Comput.*, 32(2):875–893, 2010.

[20] L. Beirão da Veiga, K. Lipnikov, and G. Manzini. Error analysis for a mimetic discretization of the steady Stokes problem on polyhedral meshes. *SIAM Journal on Numerical Analysis*, 48:1419–1443, 2010.

[21] L. Beirão da Veiga, K. Lipnikov, and G. Manzini. *The Mimetic Finite Difference Method*, volume 11 of *MS&A. Modeling, Simulations and Applications*. Springer, I edition, 2014.

[22] L. Beirão da Veiga, C. Lovadina, and D. Mora. A virtual element method for elastic and inelastic problems on polytope meshes. *Comput. Methods Appl. Mech. Engrg.*, 295:327–346, 2015.

[23] L. Beirão da Veiga, C. Lovadina, and G. Vacca. Divergence free virtual elements for the Stokes problem on polygonal meshes. *ESAIM Math. Model. Numer.*, 51(2):509–535, 2017.

[24] L. Beirão da Veiga, C. Lovadina, and G. Vacca. Virtual elements for the Navier-Stokes problem on polygonal meshes. *SIAM J. Numer. Anal.*, 56(3):1210–1242, 2018.

[25] L. Beirão da Veiga and G. Manzini. A virtual element method with arbitrary regularity. *IMA J. Numer. Anal.*, 34(2):782–799, 2014.

[26] L. Beirão da Veiga and G. Manzini. Residual a posteriori error estimation for the virtual element method for elliptic problems. *ESAIM Math. Model. Numer.*, 49:577–599, 2015.

[27] L. Beirão da Veiga, G. Manzini, and L. Mascotto. A posteriori error estimation and adaptivity in hp virtual elements. *Numer. Math.*, 143:139–175, 2019.

[28] L. Beirão da Veiga, d. Mora, and G. Vacca. The Stokes complex for virtual elements with application to Navier–Stokes flows. *J. Sci. Comput.*, 81:990–1018, 2019.

[29] M. F. Benedetto, S. Berrone, and A. Borio. The Virtual Element Method for underground flow simulations in fractured media. In *Advances in Discretization Methods*, volume 12 of *SEMA SIMAI Springer Series*, pages 167–186. Springer International Publishing, Switzerland, 2016.

[30] M. F. Benedetto, S. Berrone, S. Pieraccini, and S. Scialò. The virtual element method for discrete fracture network simulations. *Comput. Methods Appl. Mech. Engrg.*, 280(0):135 – 156, 2014.

[31] E. Benvenuti, A. Chiozzi, G. Manzini, and N. Sukumar. Extended virtual element method for the Laplace problem with singularities and discontinuities. *Comput. Methods Appl. Mech. Engrg.*, 356:571 – 597, 2019.

[32] S. Berrone and A. Borio. Orthogonal polynomials in badly shaped polygonal elements for the Virtual Element Method. *Finite Elements in Analysis & Design*, 129:14–31, 2017.

[33] S. Berrone, A. Borio, and Manzini. SUPG stabilization for the nonconforming virtual element method for advection–diffusion–reaction equations. *Comput. Methods Appl. Mech. Engrg.*, 340:500–529, 2018.

[34] S. Berrone, A. Borio, and S. Scialò. A posteriori error estimate for a PDE-constrained optimization formulation for the flow in DFNs. *SIAM J. Numer. Anal.*, 54(1):242–261, 2016.

[35] S. Berrone, S. Pieraccini, and S. Scialò. Towards effective flow simulations in realistic discrete fracture networks. *J. Comput. Phys.*, 310:181–201, 2016.

[36] S. Berrone, S. Pieraccini, S. Scialò, and F. Vicini. A parallel solver for large scale DFN flow simulations. *SIAM J. Sci. Comput.*, 37(3):C285–C306, 2015.

[37] D. Boffi, F. Brezzi, and M. Fortin. *Mixed finite element methods and applications*, volume 44. Springer, 2013.

[38] S. C. Brenner and L. R. Scott. *The mathematical theory of finite element methods*, volume 15 of *Texts in Applied Mathematics*. Springer-Verlag, New York, 1994.

[39] F. Brezzi, R. S. Falk, and L. D. Marini. Basic principles of mixed virtual element methods. *ESAIM Math. Model. Numer. Anal.*, 48(4):1227–1240, 2014.

[40] F. Brezzi, K. Lipnikov, and M. Shashkov. Convergence of mimetic finite difference method for diffusion problems on polyhedral meshes with curved faces. *Math. Models Methods Appl. Sci.*, 16(2):275–297, 2006.

[41] F. Brezzi, K. Lipnikov, M. Shashkov, and V. Simoncini. A new discretization methodology for diffusion problems on generalized polyhedral meshes. *Comput. Methods Appl. Mech. Engrg.*, 196(37–40):3682–3692, 2007.

[42] F. Brezzi and L. D. Marini. Virtual element methods for plate bending problems. *Comput. Methods Appl. Mech. Engrg.*, 253:455–462, 2013.

[43] Z. Cai, C. Tong, P. S. Vassilevski, and C. Wang. Mixed finite element methods for incompressible flow: stationary Stokes equations. *Numerical Methods for Partial Differential Equations*, 26:957–978, 2010.

[44] J. Campbell and M. Shashkov. A tensor artificial viscosity using a mimetic finite difference algorithm. *Journal of Computational Physics*, 172:739–765, 2001.

[45] A. Cangiani, E. H. Georgoulis, T. Pryer, and O. J. Sutton. A posteriori error estimates for the virtual element method. *Numer. Math.*, pages 1–37, 2017.

[46] A. Cangiani, V. Gyrya, and G. Manzini. The non-conforming virtual element method for the Stokes equations. *SIAM J. Numer. Anal.*, 54(6):3411–3435, 2016.

[47] A. Cangiani, V. Gyya, G. Manzini, and Sutton. O. Chapter 14: Virtual element methods for elliptic problems on polygonal meshes. In K. Hormann and N. Sukumar, editors, *Generalized Barycentric Coordinates in Computer Graphics and Computational Mechanics*, pages 1–20. CRC Press, Taylor & Francis Group, 2017.

[48] A. Cangiani, G. Manzini, and A. Russo. Convergence analysis of a mimetic finite difference method for elliptic problems. *SIAM J. Numer. Anal.*, 47(4):2612–2637, 2009.

[49] A. Cangiani, G. Manzini, A. Russo, and N. Sukumar. Hourglass stabilization of the virtual element method. *Int. J. Numer. Methods Eng.*, 102(3-4):404–436, 2015.

[50] A. Cangiani, G. Manzini, and O. Sutton. Conforming and nonconforming virtual element methods for elliptic problems. *IMA J. Numer. Anal.*, 37:1317–1354, 2017. (online August 2016).

[51] O. Certik, F. Gardini, G. Manzini, L. Mascotto, and G. Vacca. The p- and hp-versions of the virtual element method for elliptic eigenvalue problems. *Comput. Math. Appl.*, 2019. published online: 31 October 2019.

[52] O. Certik, F. Gardini, G. Manzini, and G. Vacca. The virtual element method for eigenvalue problems with potential terms on polytopic meshes. *Applications of Mathematics*, 63(3):333–365, 2018.

[53] M. Crouzeix and P. A. Raviart. Conforming and nonconforming finite element methods for solving the stationary Stokes equations. *RAIRO Ser. Rouge*, 7:33–75, 1973.

22

[54] D. A. Di Pietro, J. Droniou, and G. Manzini. Discontinuous skeletal gradient discretisation methods on polytopal meshes. *J. Comput. Phys.*, 355:397–425, 2018.

[55] F. Gardini, G. Manzini, and G. Vacca. The nonconforming virtual element method for eigenvalue problems. *ESAIM Math. Model. Numer.*, 53:749–774, 2019. Accepted for publication: 29 November 2018. DOI: 10.1051/m2an/2018074.

[56] V. Girault and P.-A. Raviart. *Finite Element Approximation of the Navier-Stokes Equations*, volume 749 of *Lecture Notes in Mathematics*. Springer-Verlag, Berlin, Heidelberg, 1 edition, 1979.

[57] V. Girault and P.-A. Raviart. *Finite Element Methods for Navier-Stokes Equations: Theory and Algorithms*. Springer Series in Computational Mathematics. Springer-Verlag, 1986.

[58] R. M. Höfer. Sedimentation of inertialess particles in Stokes flows. *Commun. Math. Phys.*, 360:55–10, 2018.

[59] J. Hyman and M. Shashkov. Mimetic discretizations for Maxwell's equations and the equations of magnetic diffusion. *PIER*, 32:89–121, 2001.

[60] H. Kitahata, N. Yoshinaga, K. H. Nagai, and Y. Sumino. 3 - Dynamics of Droplets. In S. Kinoshita, editor, *Pattern Formations and Oscillatory Phenomena*, pages 85–118. Elsevier, Boston, 2013.

[61] Y. Kuznetsov and S. Repin. New mixed finite element method on polygonal and polyhedral meshes. *Russian J. Numer. Anal. Math. Modelling*, 18:261–278, 2003.

[62] S. Linden, L. Cheng, and A. Wiegmann. Specialized methods for direct numerical simulations in porous media. Technical Report Report M2M-2018-01, Math2Market GmbH, Kaiserslautern, Germany, October 2018.

[63] K. Lipnikov, G. Manzini, and M. Shashkov. Mimetic finite difference method. *J. Comput. Phys.*, 257 – Part B:1163–1227, 2014. Review paper.

[64] G. Manzini, A. Russo, and N. Sukumar. New perspectives on polygonal and polyhedral finite element methods. *Math. Models Methods Appl. Sci*, 24(8):1621–1663, 2014.

[65] L. Mascotto. Ill-conditioning in the virtual element method: stabilizations and bases. *Numerical Methods for Partial Differential Equations. An International Journal*, 34(4):1258–1281, 2018.

[66] D. Mora, G. Rivera, and R. Rodríguez. A virtual element method for the Steklov eigenvalue problem. *Math. Models Methods Appl. Sci.*, 25(08):1421–1445, 2015.

[67] S. Natarajan, P. A. Bordas, and E. T. Ooi. Virtual and smoothed finite elements: a connection and its application to polygonal/polyhedral finite element methods. *International Journal on Numerical Methods in Engineering*, 104(13):1173–1199, 2015.

[68] G. H. Paulino and A. L. Gain. Bridging art and engineering using Escher-based virtual elements. *Struct. and Multidisciplinary Optim.*, 51(4):867–883, 2015.

[69] I. Perugia, P. Pietra, and A. Russo. A plane wave virtual element method for the Helmholtz problem. *ESAIM Math. Model. Num.*, 50(3):783–808, 2016.

[70] Jinshui Qin. On the convergence of some low order mixed finite elements for incompressible fluids. The Pennsylvania State University, 1994. Thesis.

[71] J. P. Smith, A. C. Barbati, S. M. Santana, J. P. Gleghorn, and B. J. Kirby. Microfluidic transport in microdevices for rare cell capture. *Electrophoresis*, 33(21):3133–3142, 2012.

[72] N. Sukumar and A. Tabarraei. Conforming polygonal finite elements. *Int. J. Numer. Methods Eng.*, 61:2045–2066, 2004.

[73] A. Tabarraei and N. Sukumar. Extended finite element method on polygonal and quadtree meshes. *Comput. Methods Appl. Mech. Engrg.*, 197:425–438, 2007.

[74] C. Talischi, G. H. Paulino, A. Pereira, and I. F. M. Menezes. Polygonal finite elements for topology optimization: A unifying paradigm. *Int. J. Numer. Methods Eng.*, 82:671–698, 2010.

[75] G. Vacca and L. Beirão da Veiga. Virtual element methods for parabolic problems on polygonal meshes. *Numer. Methods for PDEs*, 31(6):2110–2134, 2015.

[76] E. Wachspress. *Rational Bases and Generalized Barycentrics: Applications to Finite Elements and Graphics*. Technology & Engineering. Springer, 2015.

[77] P. Wriggers, W. T. Rust, and B. D. Reddy. A virtual element method for contact. *Computational Mechanics*, 58(6):1039–1050, 2016.

[78] J. Zhao, S. Chen, and B. Zhang. The nonconforming virtual element method for plate bending problems. *Math. Models Methods Appl. Sci.*, 26(9):1671–1687, 2016.

Appendix A. Approximation and orthogonality results for the virtual element method

In this appendix, we report three technical lemmas that we use in the convergence analysis of Section 4. The first two lemmas states basic results for the approximation of a vector-valued field by its virtual element interpolant and a scalar function by its polynomial projection onto the subspace of polynomials, and are presented without a proof. The interpolants $\mathbf{v}_I$ and q_I are an approximation of $\mathbf{v}$ and q, and the interpolation error can be bounded as stated in the following lemma. The third lemma presents an identity that is used in the proof of Theorem 4.1.

Lemma A.1 (Projection error [8, 38]) *Under Assumptions (M1)-(M2), for every vector-valued field $\mathbf{v} \in \left[H^{s+1}(E) \right]^2$ and scalar function $q \in H^s(E)$ with $1 \le s \le \ell$, there exists a vector polynomial $\mathbf{v}_\pi \in \left[\mathbb{P}_\ell(E) \right]^2$ and a scalar polynomial $q_\pi \in \mathbb{P}_\ell(E)$ such that*

$$||\mathbf{v} - \mathbf{v}_\pi||_{0,E} + h_E|\mathbf{v} - \mathbf{v}_\pi|_{1,E} \le Ch_E^{s+1}|\mathbf{v}|_{s+1,E}, \tag{A.1}$$

$$||q - q_\pi||_{0,E} + h_E|q - q_\pi|_{1,E} \le Ch_E^s|q|_{s,E} \tag{A.2}$$

for some positive constant C that is independent of h_E but may depend on the polynomial degree ℓ and the mesh regularity constant ϱ.

Lemma A.2 (Interpolation error [8, 38]) *Under Assumptions (M1)-(M2), for every vector-valued field $\mathbf{v} \in \left[H^{s+1}(E) \right]^2$ and scalar function $q \in H^s(E)$ with $1 \le s \le \ell$, there exists a vector valued-field $\mathbf{v}_I \in \mathbf{V}_k^h(E)$ and a scalar field $q \in Q_\ell^h$ such that*

$$||\mathbf{v} - \mathbf{v}_I||_{0,E} + h_E|\mathbf{v} - \mathbf{v}_I|_{1,E} \le Ch_E^{s+1}|\mathbf{v}|_{s+1,E}, \tag{A.3}$$

$$||q - q_I||_{0,E} + h_E|q - q_I|_{1,E} \le Ch_E^s|q|_{s,E} \tag{A.4}$$

for some positive constant C that is independent of h_E but may depend on the polynomial degree ℓ and the mesh regularity constant ϱ.

Lemma A.3 (Orthogonality between div $(\mathbf{u}_h - \mathbf{u}_I)$ and $p_h - p_I$) *Let $\mathbf{u} \in \left[H_0^1(\Omega) \right]^2$ be the exact solution of the variational formulation of the Stokes problem given in (7)-(8). Let $(\mathbf{u}_h, p_h) \in \mathbf{V}_k^h \times Q_{k-1}^h$ be the solution of the virtual element approximation (9)-(10). Then, it holds that*

$$b(\mathbf{u}_h - \mathbf{u}_I, p_h - p_I) = 0 \qquad \forall q \in Q^h. \tag{A.5}$$

Proof. First, note that the composed operator $\Pi_{k-1}^{0,E}\text{div}\,(\cdot)$ only depends on the degrees of freedom of its argument. These degrees of freedom are the same for $\mathbf{u}$ and its virtual element interpolation $\mathbf{u}_I$, so that it must hold that $\Pi_{k-1}^{0,E}\text{div}\,\mathbf{u} = \Pi_{k-1}^{0,E}\text{div}\,\mathbf{u}_I$. Using this property and the definition of the orthogonal projection $\Pi_{k-1}^{0,E}$ yield

$$b(\mathbf{u}, q) = \sum_E \int_E q\,\text{div}\,\mathbf{u}\,d\mathbf{x} = \sum_E \int_E q\Pi_{k-1}^{0,E}\text{div}\,\mathbf{u}\,d\mathbf{x} = \sum_E \int_E q\Pi_{k-1}^{0,E}\text{div}\,\mathbf{u}_I\,d\mathbf{x}$$

$$= \sum_E \int_E q\,\text{div}\,\mathbf{u}_I\,d\mathbf{x} = b(\mathbf{u}_I, q)$$

for every $q \in \mathbb{P}_{k-1}(E)$. Eventually, we note that $0 = b(\mathbf{u}, q) = b(\mathbf{u}_I, q)$ from Eq. (8) and $b(\mathbf{u}_h, q) = b_h(\mathbf{u}_h, q)$ from Eq. (30). So, it holds that $b(\mathbf{u}_h - \mathbf{u}_I, q) = 0$, and relation (A.5) immediately follows by setting $q = p_h - p_I$. □